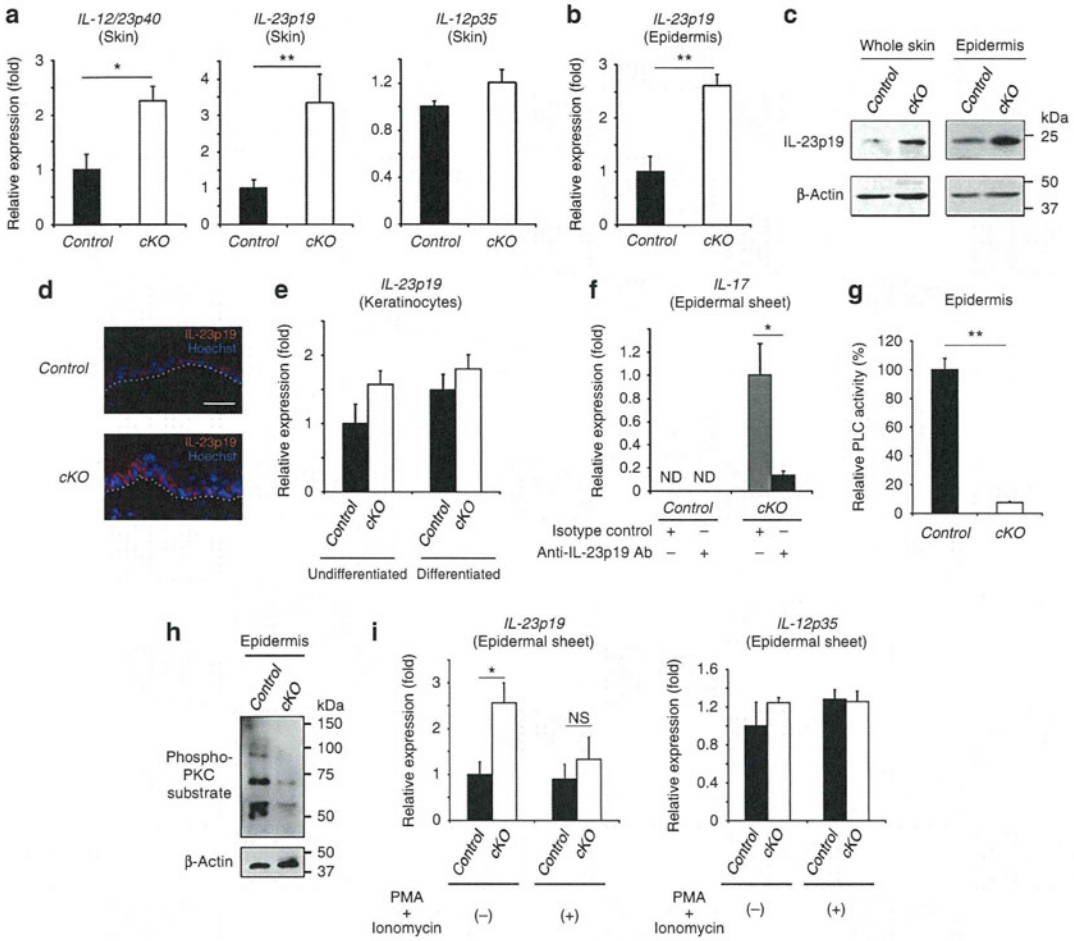

Figure 5 | IL-23 was upregulated in *cKO* skin. (**a**) *IL-12/23p40*, *IL-23p19*, and *IL-12p35* mRNA expression in the skin determined by real-time RT-PCR. All values are normalized to *GAPDH*. Results are displayed as arbitrary units (expression in control skin = 1). Mean ± s.e.m. ($n = 5$). (**b**) *IL-23p19* mRNA expression in epidermis determined by real-time RT-PCR. All values are normalized to *GAPDH*. Results are displayed as arbitrary units (expression in control = 1). Mean ± s.e.m. ($n = 6$). (**c**) Immunoblotting of IL-23p19 and β-actin in whole skin and epidermis from control and *cKO* mice. (**d**) Skin stained with the antibody against IL-23p19 (red) and Hoechst (blue). Dotted lines denote dermal-epidermal border. Scale bar, 30 μm. (**e**) *IL-23p19* mRNA expression in primary keratinocyte cultures determined by real-time RT-PCR. All values are normalized to *GAPDH*. Results are displayed as arbitrary units (expression in undifferentiated control keratinocytes = 1). Mean ± s.e.m. ($n = 3$). (**f**) Epidermal sheets were treated with anti-IL-23p19 neutralizing antibody or normal goat IgG, and *IL-17* mRNA expression was determined. All values are normalized to *GAPDH*. Results are displayed as arbitrary units (expression in *cKO* epidermal sheet treated with isotype control = 1). Mean ± s.e.m. ($n = 4$). (**g**) Relative PLC activity in epidermal lysates (PLC activity in control epidermis = 100%). Mean ± s.e.m. ($n = 4$). (**h**) Immunoblotting for phospho-PKC substrate in epidermis. β-actin was included as a loading control. (**i**) Epidermal sheets were treated with PMA and ionomycin, and mRNA expression of *IL-23p19* and *IL-12p35* was determined. All values are normalized to *GAPDH*. Results are displayed as arbitrary units (expression in control epidermal sheet without PMA/ionomycin treatment = 1). Mean ± s.e.m. ($n = 4$). Mice used in all experiments were 8–12 weeks old. Statistical significance was assessed using a Student's *t*-test. $^*P < 0.05$; $^{**}P < 0.01$. ND, not detected; NS, not significant.

activation of PLC and its downstream effector, PKC. We found that overall PLC activity was drastically decreased in *cKO* compared with control epidermis (Fig. 5g), indicating that, even in the presence of other PLC isoforms, loss of PLCδ1 impaired PLC activity in the epidermis. Consistent with the decrease in PLC activity, we found that the phosphorylation of PKC substrates was markedly decreased in cKO epidermis (Fig. 5h), indicating that loss of PLCδ1 from keratinocytes impaired the activation of the PLC downstream effector. We next determined whether the PLC downstream signal affected *IL-23* expression. PLC activation results in the generation of IP_3 and DAG, leading to elevated concentrations of intracellular calcium ions and activation of PKC. We, therefore, treated epidermal sheets with the calcium ionophore, ionomycin and phorbol 12-myristate 13-acetate (PMA), a synthetic analogue of DAG and a PKC activator, to mimic PLC activation. *IL-23p19* expression was upregulated in *cKO* epidermal sheets in the absence of ionomycin and PMA. Importantly, *IL-23p19* upregulation was ameliorated in *cKO* epidermal sheets in the presence of ionomycin and PMA (Fig. 5i). Expression of the IL-12-specific subunit, *IL-12p35*, was unchanged in the epidermis, regardless of the presence or absence of ionomycin and PMA (Fig. 5i). These results strongly suggest that *IL-23* upregulation in the *cKO* epidermis was caused by impaired PLC downstream signalling.

***cKO* skin shares features of human inflammatory skin diseases.** Because patients with human inflammatory skin diseases, such as psoriasis, show upregulation of IL-23 and IL-17 in the skin[8,32,33],

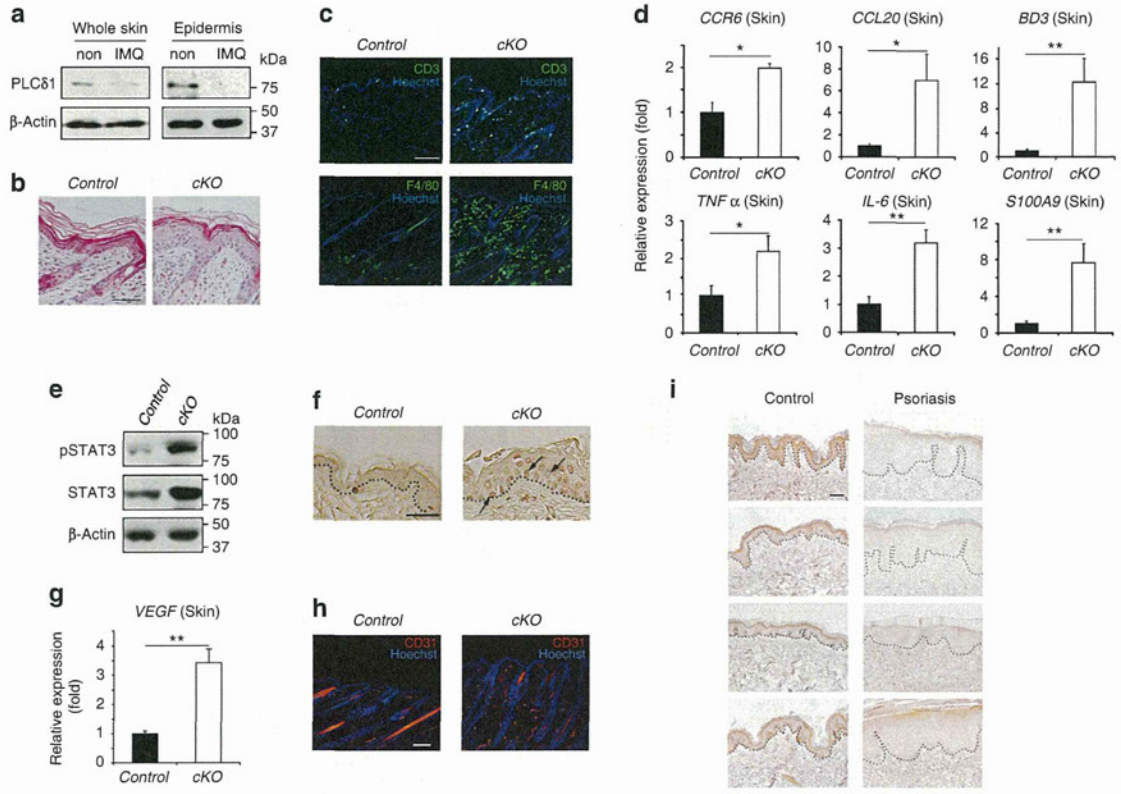

Figure 6 | *cKO* skin exhibits features of human inflammatory skin disease. (**a**) Immunoblotting of PLCδ1 and β-actin in whole skin or epidermis from non-treated (non) or IMQ-treated (IMQ) mice. (**b**) HE stained dorsal skin sections. Scale bar, 50 μm. The control skin has a normal epidermis, whereas the cKO skin has a thickened epidermis. (**c**) The skin was stained with antibodies against CD3 (green) or F4/80 (green) and Hoechst (blue). Scale bar,100 μm. (**d**) *CCR6*, *CCL20*, *β-defensin3* (*BD3*), *TNF α*, *IL-6*, and *S100A9* mRNA expression in skin determined by real-time RT-PCR. All values are normalized to *GAPDH*. Results are displayed as arbitrary units (expression in skin of control mice = 1). Mean ± s.e.m. ($n = 5$). (**e**) Immunoblotting for total and phosphorylated STAT3 (pSTAT3) in skin. β-actin was included as a loading control. (**f**) Skin stained with antibody against phosphorylated STAT3. Dotted lines denote dermal-epidermal border. Scale bar, 20 μm. Nuclear staining of phosphorylated STAT3 is indicated by arrows. (**g**) *VEGF* mRNA expression in skin determined by real-time RT-PCR. All values are normalized to *GAPDH*. Results are displayed as arbitrary units (expression in skin of control mice = 1). Mean ± s.e.m. ($n = 5$). (**h**) Skin stained with the antibody against CD31 (red) and Hoechst (blue). Hair shafts show nonspecific autofluorescence (red). Scale bar, 100 μm. (**i**) Skin from four non-psoriatic volunteers and four patients with psoriasis were stained with antibody against human PLCδ1 (brown). Dotted lines denote dermal-epidermal border. Scale bar, 100 μm. Body sites of each skin samples were as follows: control; arm, waist, back, and back (indicated from the top panel to the bottom panel). Psoriasis; arm, abdominal, leg, and leg (indicated from the top panel to the bottom panel). (**a**, **c**–**h**) 8–12-week-old mice were used. (**b**–**h**) Untreated IMQs were used. The data presented in (**b**, **c**, **e**, **f**, **h**) are representative of analyses of three mice per genotype. The data presented in (**a**) is representative of analyses of two mice per genotype. Statistical significance was assessed using a Student's *t*-test. $^*P < 0.05$; $^{**}P < 0.01$.

PLCδ1 could be involved in pathogenesis of these diseases. We therefore, examined PLCδ1 expression in the topical imiquimod (IMQ)-induced psoriasiform lesion, which is a mouse model of human psoriasis[34]. Interestingly, PLCδ1 protein was decreased in IMQ-treated skin compared with non-treated skin (Fig. 6a). PLCδ1 downregulation was also observed in the epidermis of IMQ-treated mice (Fig. 6a). These observations strongly suggest that epidermal PLCδ1 is implicated in a mouse model of human psoriasis. We next determined whether *cKO* skin shares features of human inflammatory skin diseases. Histological analysis revealed that *cKO* skin showed acanthosis (Fig. 6b) and infiltration of immune cells (Fig. 6c), as seen in human inflammatory skin diseases, such as psoriasis. In addition, *cKO* epidermis displayed abnormal patterns of differentiation marker expression, including the interfollicular expression of K6 (Supplementary Fig. S12), which is observed in human inflammatory skin diseases. Real-time RT–PCR showed that inflammatory genes upregulated in human inflammatory skin diseases are also upregulated in *cKO* skin (Fig. 6d)[35–40]. Activation of the signal transducer and activator of transcription 3 (STAT3) is also a feature of psoriasis[41], and western blotting revealed that both total and phosphorylated STAT3 proteins were increased in *cKO* skin (Fig. 6e). Consistent with these results, immunohistochemistry detected phosphorylated STAT3 in the nuclei of the *cKO* epidermis (Fig. 6f). Because the dermis is highly vascularized in some skin diseases[42–45], we analysed the expression levels of the potent angiogenic factor, *vascular endothelial growth factor (VEGF)*. *VEGF* upregulation was observed in *cKO* skin (Fig. 6g). In addition, immunofluorescence revealed that *cKO* skin was highly vascularized (Fig. 6h), in a manner similar to that in human inflammatory skin diseases. Most phenotypes in *cKO* skin were also observed in a mouse model of human psoriasis (Supplementary Fig. S13). Interestingly, PLCδ1 protein was downregulated in epidermis of human psoriatic skin (Fig. 6i). These observations strongly suggest that epidermal PLCδ1 is involved in human psoriasis.

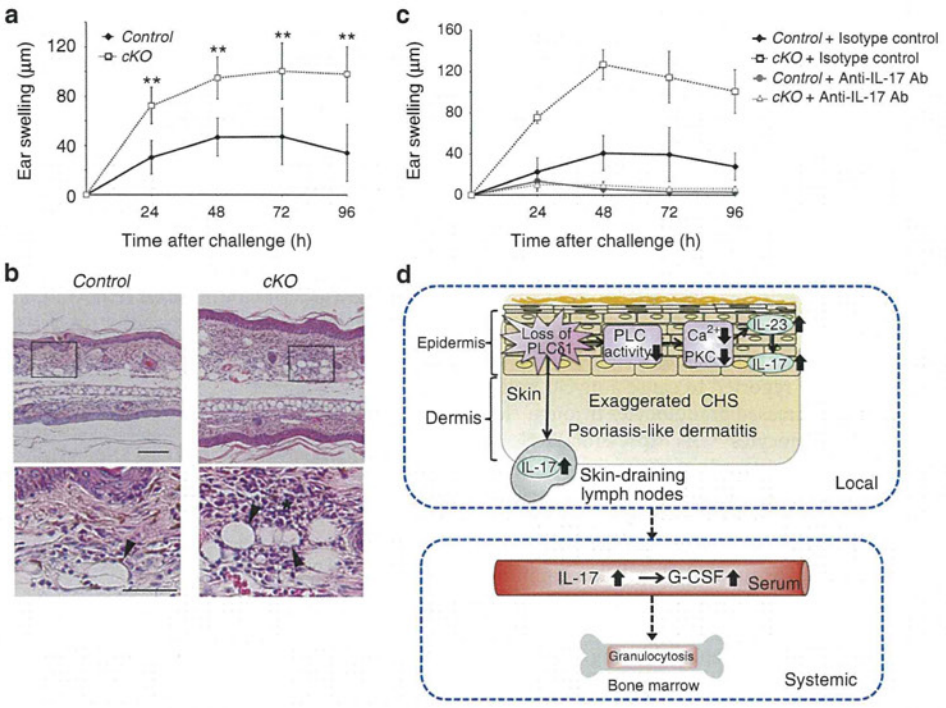

Figure 7 | Loss of PLCδ1 in keratinocytes exaggerates CHS responses. (**a**) Time course of ear swelling after DNFB challenge. Ear swelling was measured at the indicated times. Mean±s.d. ($n=4$). (**b**) HE stains of ear after DNFB challenge. The ears of sensitized mice were painted with DNFB, collected 96 h later and stained with HE. Lower panels are magnified views of the boxed regions in the upper panels. Scale bar in upper panel, 100 μm. Scale bar in lower panel, 50 μm. (**c**) Sensitized mice were treated with anti-IL-17 neutralizing antibody or normal rat IgG before challenge, and ear swelling was measured at the indicated times. Mean±s.d. ($n=3$). Mice used in all experiments were 8–12 weeks old. The data presented in (**b**) are representative of three mice per genotype. Statistical significance was assessed using a Student's *t*-test. $^{**}P<0.01$. (**d**) Proposed model of local and systemic phenotypes induced by epidermal loss of PLCδ1. Epidermal loss of PLCδ1 impairs overall PLC activity and activation of PLC downstream signals, which causes increased production of IL-23 in the epidermis and whole skin. IL-23 induces IL-17 production in the epidermis. IL-17 was also overproduced in the skin-draining lymph nodes. This aberrant activation of the local IL-23/IL-17 axis resulted in a phenotype similar to that in human psoriasis and exaggerated CHS responses. Regarding systemic phenotypes, serum IL-17 levels were increased presumably as a result of skin and/or skin-draining lymph node-derived IL-17 (dotted arrow). Elevated serum IL-17 concentrations likely cause subsequent granulocytosis through G-CSF production (dotted arrow).

PLCδ1 in keratinocytes influences contact hypersensitivity. Dinitrofluorobenzene (DNFB)-induced contact hypersensitivity (CHS) of the skin in mice is commonly used as a model for studying the pathogenesis of allergic contact dermatitis (ACD), in which IL-17 has a critical role[4,46]. We, therefore, assessed CHS responses in *cKO* mice. Mice were sensitized and challenged with DNFB, and the CHS response was assessed by measuring ear swelling. On challenge with DNFB, DNFB-sensitized control mice exhibited a CHS response with mild ear swelling, whereas *cKO* mice showed more prominent ear swelling with exaggerated edema and severe inflammatory cell infiltration (Fig. 7a,b). Interestingly, IL-17 neutralization resulted in abrogation of the exaggerated ear swelling in *cKO* mice almost to basal level at any time after challenge (Fig. 7c). These results indicate that the exacerbated CHS in *cKO* mice was IL-17-dependent.

Discussion

In all of our mouse models, the level of expression of PLCδ1 in keratinocytes was inversely correlated with the levels of expression of IL-23 and IL-17 in skin and skin-draining LNs. Thus, loss of PLCδ1 in keratinocytes results in local activation of the IL-23/IL-17 axis (Fig. 7d). Keratinocytes from lesional psoriatic skin express IL-23 (ref. 32). In addition, human keratinocytes stimulated with nickel, a common hapten inducing CHS, produce IL-23 (ref. 47). These results are consistent with our observation that *IL-23p19* was upregulated in keratinocytes of cKO epidermis (Fig. 5d). Because IL-23p19 was upregulated mainly in basal layer of cKO interfollicular epidermis (Fig. 5d), essential and sufficient roles of suprabasal PLCδ1 in maintenance of normal IL-23p19 levels (Fig. 3d; Supplementary Fig. S11) is somewhat surprising. Interactions between suprabasal and basal keratinocytes might be important in regulation of IL-23p19 expression. We also found that γδ T cells in cKO epidermis expressed *IL-17* (Supplementary Fig. S9). Interestingly, γδ T cells were recently reported to be major IL-17 producers in skin of IL-23-mediated psoriasiform dermatitis[48,49].

Aberrant activation of the IL-23/IL-17 axis in the skin is known to be involved in the development of inflammatory human skin diseases, especially psoriasis[8]. Indeed, IL-23 injection into normal skin was sufficient for the development of psoriatic phenotypes in mice[50,51], and a monoclonal antibody against IL-12/23p40 subunit, ustekinumab is efficacious for the treatment of patients with moderate-to-severe psoriasis[52]. Although *cKO* skin shared some molecular features of psoriasis, it did not demonstrate all the histological characteristics of psoriatic skin. This may be because the expression of another key cytokine for the development of psoriasis, IL-22, was not upregulated in *cKO* skin (data not shown). Nonetheless, as PLCδ1 expression was decreased in the epidermis of patients with psoriasis (Fig. 6i) and in mouse IMQ-induced psoriasiform lesion (Fig. 6a), PLCδ1 may be involved in the pathogenesis of psoriasis. *cKO* mice also demonstrated increased sensitivity to hapten-induced

CHS, a mouse model of human ACD. The fact that the exaggerated CHS response in *cKO* mice was inhibited by IL-17 neutralization demonstrated the involvement of PLCδ1 in IL-17-mediated ACD.

Keratinocyte-specific ablation of PLCδ1 also caused systemic elevation of IL-17 and granulocytosis. Because activation of the local IL-23/IL-17 axis and systemic granulocytosis were both observed in *cKO*, but not in *Tg/KO* mice, the absence of epidermal PLCδ1, local IL-23/IL-17 axis activation, and systemic granulocytosis were strongly correlated with each other. This strict correlation strongly suggests that activation of the local IL-23/IL-17 axis and elevation of serum IL-17 and G-CSF concentrations are likely to be responsible for granulocytosis. On the basis of previous findings[53], the serum concentrations of IL-17 and G-CSF in *PLCδ1* $^{-/-}$ and *cKO* mice were sufficient to produce a systemic increase in granulocytes. The loss of JunB in keratinocytes was recently reported to cause a myeloproliferative disease characterized by increased granulocytes through elevated G-CSF production by keratinocytes[54]. As expression levels of *JunB* and *G-CSF* were unaltered in epidermis of *cKO* mice (data not shown), PLCδ1 seems to cause granulocytosis by a different mechanism to that observed in keratinocyte-specific *JunB*-knockout mice.

The results of this study demonstrate that disruption of the *PLCδ1* gene in keratinocytes disturbs not only local skin immune responses, but also the systemic homeostasis of haematopoietic cells, especially granulocytes. The proposed mechanism underlying the phenotypes seen in *cKO* mice is depicted in Fig. 7d. These findings suggest that targeting body-surface-specific inflammatory pathways may prevent not only inflammatory skin diseases but systemic granulocytosis and related disorders too.

Methods

Mice. *PLCδ1* $^{-/-}$ mice and *PLCδ1 flox/flox* mice (Acc. No. CDB0552K: http://www.cdb.riken.jp/arg/mutant%20mice%20list.html) were produced as described[55] (http://www.cdb.riken.jp/arg/Methods.html). In brief, a floxed allele of *PLCδ1* was generated by inserting loxP sites upstream of exon 4 and downstream of exon 5. The resulting mutant mice carrying the floxed allele of *PLCδ1* were crossed with *B6-Tg (CAG-FLPe)36* mice (RIKEN BRC, RBRCO 1834) to remove the neomycin-resistant cassette, and then with K14-Cre transgenic mice[56] (#004782, Jackson Laboratory, Bar Harbor, ME, USA) to remove the floxed exons. *Foxn1::PLCδ1* transgenic mice (Acc. No. CDB0437T: http://www.cdb.riken.jp/arg/TG%20mutant%20mice%20list.html) were developed as per a standard protocol. In brief, murine *PLCδ1* was subcloned into a plasmid that contained a 27,970-bp *Foxn1* promoter fragment (gift from Dr T. Boehm)[57]. The construct was linearized and injected into C57BL/6N or BDF1 pronuclei according to standard protocols. *Tg/KO* mice were generated with two independent transgenic mouse lines. Adult mice or pups were routinely genotyped by PCR. The primer sequences used are listed in Supplementary Table S4. Age- and sex-matched littermates were used to minimize any effects of genetic background. All animal studies were approved by the animal experiments review board of Tokyo University of Pharmacy and Life Sciences.

FACS analysis of cells from peripheral blood and tissues. Fluorophor-conjugated monoclonal antibodies were used in various combinations to stain peripheral blood mononuclear cells, splenocytes, and bone marrow. Red blood cells were depleted with 1×RBC Lysis Buffer (eBioscience, San Diego, CA, USA). For staining, 2–5×10^6 cells were used. Fc receptor was blocked by CD16/32 antibody. After staining (Supplementary Table S5), the cells were fixed with 1% paraformaldehyde. Stained and fixed cells were assayed using a FACSCanto flow cytometer (BD Biosciences) and further analysed with FlowJo software (Tree Star, Ashland, OR, USA).

BrdU incorporation assay. Analysis of *in vivo* BrdU incorporation into immature granulocytes was performed using the BrdU Flow Kit (BD Pharmingen) after intraperitoneal injection of 1.5 mg of BrdU. Mice were killed 1 h later and the bone marrow cells were collected. Cell surface markers were identified using Gr-1 and CD11b antibodies.

Colony-forming unit assays. Colony-forming cell assays were performed using bone marrow cells and MethoCult M3434 (Stem Cell Technologies, Vancouver, British Columbia, Canada). Colonies were counted after 12 days' incubation in a humidified atmosphere with 5% CO_2 and characterized according to their unique morphologies.

Bone marrow transplantation. Recipient mice were irradiated with 9 Gy whole-body irradiation. Donors were *PLCδ1* $^{+/-}$ or *PLCδ1* $^{-/-}$ (CD45.2$^+$) mice, while recipients were of B6.SJL (CD45.1$^+$) background. A total of 4×10^6 donor bone marrow cells were intravenously injected into each recipient. Peripheral blood, spleen, and bone marrow chimerism were analysed by immunostaining for CD45 congenic marker isoforms in leukocytes 1 month after transplantation.

Intracellular IL-17 staining. Cells from ILNs and MLNs were cultured for 4 h in RPMI-1640 (Invitrogen) containing 10% fetal bovine serum (FBS) in the presence of PMA (50 ng ml^{-1}; Sigma) and ionomycin (1 μg ml^{-1}; Invitrogen). Brefeldin A (10 μg ml^{-1}; Sigma) was added for the last 2 h of incubation. Cells were collected and stained with antibodies (Supplementary Table S5) against cell surface antigens. The cells were then subjected to intracellular cytokine staining using the mouse Foxp3 buffer set (BD Pharmingen), according to the manufacturer's instructions.

Enzyme-linked immunosorbent assays (ELISA). Serum G-CSF and IL-17 levels were determined using the Quantikine Mouse G-CSF and IL-17 Immunoassay kits (R&D Systems, Minneapolis, MN, USA), respectively, according to the manufacturer's instructions.

Real-time RT-PCR. Total RNA was isolated using the RNeasy Mini kit (Qiagen, Hilden, Germany), according to the manufacturer's protocol. Template complementary DNA was synthesized from total RNA using the QuantiTect Reverse Transcription kit (Qiagen) or the ReverTra Ace qPCR RT kit (Toyobo, Osaka, Japan). Real-time PCR was performed using the THUNDERBIRD SYBR qPCR Mix (Toyobo) in a CFX96 thermocycler (Bio-Rad, München, Germany). Primer sequences are listed in Supplementary Table S4. The relative amounts of mRNA were normalized to glyceraldehyde 3-phosphate dehydrogenase mRNA.

Immunofluorescence and immunohistochemistry. Immunofluorescence analysis for IL-23p19, CD3, F4/80, CD31, K1, K5, K6, and Loricrin was performed using frozen sections. Briefly, sections were fixed in acetone (for IL-23p19) or 2% paraformaldehyde (for CD3, F4/80, CD31, K1, K5, K6 and Loricrin), and nonspecific binding sites were blocked with TNB (PerkinElmer, Waltham, MA, USA). The sections were then incubated with primary antibodies (Supplementary Table S5). Antibody binding was detected by subsequent incubation of the sections with Alexa Fluor 488 or 568-conjugated secondary antibody. Counter-staining was performed with Hoechst 33258 (Invitrogen). Immunofluorescence analysis of mouse PLCδ1 was performed using paraffin sections with TSA Plus Cyanine 3 System (PerkinElmer). Sections were observed under a BZ-8000 microscope (Keyence, Tokyo, Japan). Immunohistochemistry for phosphorylated STAT3 was carried out on paraffin sections, according to the manufacturer's instructions. Immunohistochemical assays for human PLCδ1 were performed using paraffin sections with a Vectastain Elite rabbit ABC kit (Vector Laboratories, Burlingame, CA, USA). Sections were examined under a BX51 microscope (Olympus, Tokyo, Japan).

Measurement of PLC activity. Epidermis was homogenized in 40 mM HEPES-KOH, pH 7.0, 120 mM KCl containing 0.1% sodium deoxycholate. The PLC activity of these epidermal lysates was assayed by hydrolysis of $PI(4,5)P_2$ in a 50-μl reaction mixture containing 20,000 d.p.m. of [3H]PI(4,5)P2 (PerkinElmer Life Sciences), 40 μM $PI(4,5)P_2$, and 50 μM phosphatidylethanolamine as phospholipids micelles. The micelles were incubated with epidermal lystaes at 37 °C for 5 min, and the reaction was stopped by adding chloroform/methanol (2:1, v/v). Radioactive IP_3 was extracted with 1 N HCl, and radioactivity in the upper aqueous phase was measured for 1 min in a liquid scintillation counter[58].

Hapten-induced CHS. Mice were sensitized with DNFB (Sigma) by painting the shaved dorsal skin with 50 μl of 0.5% (w/v) DNFB dissolved in acetone:olive oil (4:1). Five days later, 10 μl of 0.2% (w/v) DNFB was applied to both sides of the right ear. The same volume of acetone:olive oil (4:1) was applied to the left ear as an unchallenged control. Ear swelling was calculated by subtracting the thickness of the left ear from that of the right ear after measurement with a pair of callipers. To detect the role of IL-17 in the elicitation of CHS, mice were sensitized and treated twice intraperitoneally with anti-IL-17 antibody (R&D Systems) (200 μg per mouse) or normal rat IgG (R&D Systems) (200 μg per mouse) on days 4 and 5, after sensitization. Mice were challenged on day 5 and CHS was measured.

Explant culture of epidermal sheet. Ear or tail skin was removed from adult mice and incubated for 30 min at 37 °C in 0.25% trypsin (Invitrogen) to separate the epidermis from the dermis. For stimulation with PMA and ionomycin, epidermal sheets were cultured for 6 h in RPMI-1640 containing 10% FBS with or without PMA (100 ng ml^{-1}) and ionomycin (2.5 μg ml^{-1}). For IL-23 neutralization, epidermal sheets were cultured for 24 h in RPMI-1640 containing 10% FBS with 4 μg of anti-IL-23p19 antibody (R&D Systems) or normal goat IgG (R&D Systems).

G-CSF induction. Swiss 3T3 cells were maintained in DMEM containing 10% FBS. Cells isolated from skin-draining lymph nodes were cultured for 48 h in RPMI-1640 containing 10% FBS and CM was collected. Swiss 3T3 cells were cultured for 24 h in DMEM containing 10% FBS and skin-draining lymph-node CM. Skin-draining lymph-node CM was preincubated with anti-IL-17 antibody (1 μg ml^{-1}) or normal rat IgG for 1 h before adding to Swiss 3T3 cells.

Intracellular IL-17 staining of epidermal single-cell preparation. Ear skin was removed from adult mice and incubated for 1 h at 37 °C in 0.5% trypsin to separate the epidermis from the dermis. Single-cell suspensions were prepared from the epidermis by incubation for an additional 15 min with 0.5% trypsin. Leukocyte enrichment was performed by overlaying a single-cell suspension on a Percoll density gradient and centrifuging. Epidermal cell suspensions were then stained with antibodies against CD3, and the cells were subjected to intracellular IL-17 staining using the mouse Foxp3 buffer set, according to the manufacturer's instructions.

IMQ treatment. Balb/c mice were treated on the shaved back skin or inner side of the right ear with a daily topical dose of 62.5 or 12.5 mg of commercially available IMQ cream (5%) (Beselna Cream; Mochida Pharmaceuticals, Tokyo, Japan) for 6 days, respectively. Left ears were untreated and used as control. Back skin or ears were collected 24 h after the last treatment. For the preparation of epidermal samples, ear skin was incubated for 30 min at 37 °C in 0.25% trypsin to separate the epidermis from the dermis.

Human subjects. Patients with psoriasis and healthy volunteers without psoriasis were enrolled. Informed consent was obtained from all participants. The study protocol was approved by the Ethics Committee of Kyoto University and was conducted according to the Declaration of Helsinki Principles. Skin biopsies were analysed by immunohistochemistry.

References

1. Berridge, M. J. & Irvine, R. F. Inositol trisphosphate, a novel second messenger in cellular signal transduction. *Nature* **312,** 315–321 (1984).
2. Nishizuka, Y. The molecular heterogeneity of protein kinase C and its implications for cellular regulation. *Nature* **334,** 661–665 (1988).
3. Suh, P. G. *et al.* Multiple roles of phosphoinositide-specific phospholipase C isozymes. *BMB Rep.* **41,** 415–434 (2008).
4. Nakae, S. *et al.* Antigen-specific T cell sensitization is impaired in IL-17-deficient mice, causing suppression of allergic cellular and humoral responses. *Immunity* **17,** 375–387 (2002).
5. Goverman, J. Autoimmune T cell responses in the central nervous system. *Nat. Rev. Immunol.* **9,** 393–407 (2009).
6. Lubberts, E. *et al.* Requirement of IL-17 receptor signaling in radiation-resistant cells in the joint for full progression of destructive synovitis. *J. Immunol.* **175,** 3360–3368 (2005).
7. Nakae, S., Nambu, A., Sudo, K. & Iwakura, Y. Suppression of immune induction of collagen-induced arthritis in IL-17-deficient mice. *J. Immunol.* **171,** 6173–6177 (2003).
8. Lee, E. *et al.* Increased expression of interleukin 23 p19 and p40 in lesional skin of patients with psoriasis vulgaris. *J. Exp. Med.* **199,** 125–130 (2004).
9. Fujino, S. *et al.* Increased expression of interleukin 17 in inflammatory bowel disease. *GUT* **52,** 65–70 (2003).
10. Yen, D. *et al.* IL-23 is essential for T cell-mediated colitis and promotes inflammation via IL-17 and IL-6. *J. Clin. Invest.* **116,** 1310–1316 (2006).
11. Aggarwal, S., Ghilardi, N., Xie, M. H., de Sauvage, F. J. & Gurney, A. L. Interleukin-23 promotes a distinct CD4 T cell activation state characterized by the production of interleukin-17. *J. Biol. Chem.* **278,** 1910–1914 (2003).
12. Happel, K. I. *et al.* Roles of Toll-like receptor 4 and IL-23 in IL-17 expression in response to Klebsiella pneumoniae infection. *J. Immunol.* **170,** 4432–4436 (2003).
13. Forlow, S. B. *et al.* Increased granulopoiesis through interleukin-17 and granulocyte colony-stimulating factor in leukocyte adhesion molecule-deficient mice. *Blood* **98,** 3309–3314 (2001).
14. Schwarzenberger, P. *et al.* IL-17 stimulates granulopoiesis in mice: use of an alternate, novel gene therapy-derived method for *in vivo* evaluation of cytokines. *J. Immunol.* **161,** 6383–6389 (1998).
15. Schwarzenberger, P. *et al.* Requirement of endogenous stem cell factor and granulocyte-colony-stimulating factor for IL-17-mediated granulopoiesis. *J. Immunol.* **164,** 4783–4789 (2000).
16. Fried, L. *et al.* Inflammatory and prothrombotic markers and the progression of renal disease in elderly individuals. *J. Am. Soc. Nephrol.* **15,** 3184–3191 (2004).
17. Margolis, K. L. *et al.* Leukocyte count as a predictor of cardiovascular events and mortality in postmenopausal women: the Women's Health Initiative Observational Study. *Arch. Intern. Med.* **165,** 500–508 (2005).
18. Ruggiero, C. *et al.* White blood cell count and mortality in the Baltimore Longitudinal Study of Aging. *J. Am. Coll. Cardiol.* **49,** 1841–1850 (2007).
19. Nakamura, Y. *et al.* Phospholipase C-δ1 and -δ3 are essential in the trophoblast for placental development. *Mol. Cell. Biol.* **25,** 10979–10988 (2005).
20. Ichinohe, M. *et al.* Lack of phospholipase C-delta1 induces skin inflammation. *Biochem. Biophys. Res. Commun.* **356,** 912–918 (2007).
21. Swamy, M., Jamora, C., Havran, W. & Hayday, A. Epithelial decision makers: in search of the 'epimmunome'. *Nat. Immunol.* **11,** 656–665 (2010).
22. Nestle, F. O., Di Meglio, P., Qin, J. Z. & Nickoloff, B. J. Skin immune sentinels in health and disease. *Nat. Rev. Immunol.* **9,** 679–691 (2009).
23. Xiao, W. *et al.* Tumor suppression by phospholipase C-β3 via SHP-1-mediated dephosphorylation of Stat5. *Cancer Cell* **16,** 161–171 (2009).
24. Guo, Y., Rebecchi, M. & Scarlata, S. Phospholipase Cbeta2 binds to and inhibits phospholipase Cdelta1. *J. Biol. Chem.* **280,** 1438–1447 (2005).
25. Ueda, Y., Kondo, M. & Kelsoe, G. Inflammation and the reciprocal production of granulocytes and lymphocytes in bone marrow. *J. Exp. Med.* **201,** 1771–1780 (2005).
26. Walkley, C. R. *et al.* A microenvironment-induced myeloproliferative syndrome caused by retinoic acid receptor gamma deficiency. *Cell* **129,** 1097–1110 (2007).
27. Yang, L. *et al.* Cdc42 critically regulates the balance between myelopoiesis and erythropoiesis. *Blood* **110,** 3853–3861 (2007).
28. Walkley, C. R., Yuan, Y. D., Chandraratna, R. A. & McArthur, G. A. Retinoic acid receptor antagonism *in vivo* expands the numbers of precursor cells during granulopoiesis. *Leukemia* **16,** 1763–1772 (2002).
29. Nakamura, Y. *et al.* Phospholipase C-δ1 is an essential molecule downstream of Foxn1, the gene responsible for the nude mutation, in normal hair development. *FASEB J.* **22,** 841–849 (2008).
30. Lee, D., Prowse, D. M. & Brissette, J. L. Association between mouse nude gene expression and the initiation of epithelial terminal differentiation. *Dev. Biol.* **208,** 362–374 (1999).
31. Oppmann, B. *et al.* Novel p19 protein engages IL-12p40 to form a cytokine, IL-23, with biological activities similar as well as distinct from IL-12. *Immunity* **13,** 715–725 (2000).
32. Johansen, C. *et al.* Characterization of the interleukin-17 isoforms and receptors in lesional psoriatic skin. *Br. J. Dermatol.* **160,** 319–324 (2009).
33. Piskin, G., Sylva-Steenland, R. M., Bos, J. D. & Teunissen, M. B. *In vitro* and *in situ* expression of IL-23 by keratinocytes in healthy skin and psoriasis lesions: enhanced expression in psoriatic skin. *J. Immunol.* **176,** 1908–1915 (2006).
34. van der Fits, L. *et al.* Imiquimod-induced psoriasis-like skin inflammation in mice is mediated via the IL-23/IL-17 axis. *J Immunol.* **182,** 5836–5845 (2009).
35. Homey, B. *et al.* Up-regulation of macrophage inflammatory protein-3 alpha/CCL20 and CC chemokine receptor 6 in psoriasis. *J. Immunol.* **164,** 6621–6632 (2000).
36. Ong, P. Y. *et al.* Endogenous antimicrobial peptides and skin infections in atopic dermatitis. *N. Engl. J. Med.* **347,** 1151–1160 (2002).
37. Wilson, N. J. *et al.* Development, cytokine profile and function of human interleukin 17-producing helper T cells. *Nat. Immunol.* **8,** 950–957 (2007).
38. Ettehadi, P. *et al.* Elevated tumour necrosis factor-alpha (TNF-alpha) biological activity in psoriatic skin lesions. *Clin. Exp. Immunol.* **96,** 146–151 (1994).
39. Grossman, R. M. *et al.* Interleukin 6 is expressed in high levels in psoriatic skin and stimulates proliferation of cultured human keratinocytes. *Proc. Natl Acad. Sci. USA* **86,** 6367–6371 (1989).
40. Broome, A. M., Ryan, D. & Eckert, R. L. S100 protein subcellular localization during epidermal differentiation and psoriasis. *J. Histochem. Cytochem.* **51,** 675–685 (2003).
41. Sano, S. *et al.* Stat3 links activated keratinocytes and immunocytes required for development of psoriasis in a novel transgenic mouse model. *Nat. Med.* **11,** 43–49 (2005).
42. Creamer, D., Allen, M. H., Sousa, A., Poston, R. & Barke, J. N. Localization of endothelial proliferation and microvascular expansion in active plaque psoriasis. *Br. J. Dermatol.* **136,** 859–865 (1997).
43. Hern, S., Stanton, A. W., Mellor, R., Levick, J. R. & Mortimer, P. S. Control of cutaneous blood vessels in psoriatic plaques. *J. Invest. Dermatol.* **113,** 127–132 (1999).
44. Murphy, M., Kerr, P. & Grant-Kels, J. M. The histopathologic spectrum of psoriasis. *Clin. Dermatol.* **25,** 524–528 (2007).
45. Micali, G., Lacarrubba, F., Musumeci, M. L., Massimino, D. & Nasca, M. R. Cutaneous vascular patterns in psoriasis. *Int. J. Dermatol.* **49,** 249–56 (2010).
46. He, D. *et al.* IL-17 and IFN-γ mediate the elicitation of contact hypersensitivity responses by different mechanisms and both are required for optimal responses. *J. Immunol.* **183,** 21463–21470 (2009).
47. Larsen, J. M., Bonefeld, C. M., Poulsen, S. S., Geisler, C. & Skov, L. IL-23 and T(H)17-mediated inflammation in human allergic contact dermatitis. *J. Allergy Clin. Immunol.* **123,** 486–492 (2009).
48. Cai, Y. *et al.* Pivotal role of dermal IL-17-producing γδ T cells in skin inflammation. *Immunity,* **4,** 596–610 (2011).
49. Mabuchi, T., Takekoshi, T. & Hwang, S. T. Epidermal CCR6+ γδ T cells are major producers of IL-22 and IL-17 in a murine model of Psoriasiform dermatitis. *J. Immunol.* **187,** 5026–5031 (2011).
50. Hedrick, M. N. *et al.* CCR6 is required for IL-23–induced psoriasis-like inflammation in mice. *J. Clin. Invest.* **119,** 2317–2329 (2009).
51. Zheng, Y. *et al.* Interleukin-22, a T(H)17 cytokine, mediates IL-23-induced dermal inflammation and acanthosis. *Nature.* **445,** 648–651 (2007).
52. Leonardi, C. L. *et al.* Efficacy and safety of ustekinumab, a human interleukin-12/23 monoclonal antibody, in patients with psoriasis: 76-week results from a randomized, double-blind, placebo-controlled trial (PHOENIX 1). *The Lancet.* **371,** 1665–1674 (2008).

53. Shigeta, A. *et al.* An L-selectin ligand distinct from P-selectin glycoprotein ligand-1 is expressed on endothelial cells and promotes neutrophil rolling in inflammation. *Blood* **13,** 4915–4923 (2008).
54. Meixner, A. *et al.* Epidermal JunB represses G-CSF transcription and affects haematopoiesis and bone formation. *Nat. Cell Biol.* **10,** 1003–1011 (2008).
55. Nakamura, Y. *et al.* Phospholipase Cdelta1 is required for skin stem cell lineage commitment. *EMBO J.* **22,** 2981–2991 (2003).
56. Dassule, H. R., Lewis, P., Bei, M., Maas, R. & McMahon, A. P. Sonic hedgehog regulates growth and morphogenesis of the tooth. *Development.* **127,** 4775–4785 (2000).
57. Bleul, C.C. & Boehm, T. BMP signaling is required for normal thymus development. *J. Immunol.* **175,** 5213–5221 (2005).
58. Kouchi, Z. *et al.* Phospholipase Cdelta3 regulates RhoA/Rho kinase signaling and neurite outgrowth. *J. Biol. Chem.* **286,** 8459–8471 (2011).

Acknowledgements

We thank Dr. Z. Kouchi, R. Fujimori, and Y. Hashimoto for technical assistances and fruitful discussions. We also thank Dr. T. Boehm for providing the *Foxn1* promoter construct. This work was supported by a Grant-in-Aid for Scientific Research (B), the Funding Program for Next Generation World-Leading Researchers, the Mochida Memorial Foundation for Medical and Pharmaceutical Research and the Takeda Science Foundation to K.F., as well as a Grant-in-Aid for Young Scientists (B) to Y.N. K. Kanemaru is supported by a predoctoral fellowship from the Japan Society of the Promotion of Sciences.

Author contributions

K. Kanemaru, Y.N., K.F. designed the experiments; K. Kanemaru, Y.N., K.S., R.K., S.T., M.Y., M.I., H.K., G.S., K. Kabashima and K.N. performed experiments; K. Kanemaru, Y.N., K.F., K.S., M.A., H.Y. and C.J. analysed data; K. Kanemaru, Y.N. and K.F. wrote the paper.

Additional information

Supplementary Information accompanies this paper at http://www.nature.com/naturecommunications

Competing financial interests: The authors declare no competing financial interests.

Reprints and permission information is available online at http://npg.nature.com/reprintsandpermissions/

How to cite this article: Kanemaru, K. *et al.* Epidermal phospholipase Cδ1 regulates granulocyte counts and systemic interleukin-17 levels in mice. *Nat. Commun.* 3:963 doi: 10.1038/ncomms1960 (2012).

Protection from liver fibrosis by a peroxisome proliferator-activated receptor δ agonist

Keiko Iwaisako[a,b], Michael Haimerl[a], Yong-Han Paik[a,c], Kojiro Taura[a], Yuzo Kodama[a], Claude Sirlin[b], Elizabeth Yu[d], Ruth T. Yu[d], Michael Downes[d], Ronald M. Evans[d,1], David A. Brenner[a], and Bernd Schnabl[a,1]

Departments of [a]Medicine and [b]Radiology, University of California at San Diego, La Jolla, CA 92093; [c]Department of Internal Medicine, Samsung Medical Center, Sungkyunkwan University School of Medicine, Seoul 135-710, Korea; and [d]Gene Expression Laboratory, Salk Institute for Biological Studies, La Jolla, CA 92037

Contributed by Ronald M. Evans, March 28, 2012 (sent for review November 18, 2011)

Peroxisome proliferator-activated receptor delta (PPARδ), a member of the nuclear receptor family, is emerging as a key metabolic regulator with pleiotropic actions on various tissues including fat, skeletal muscle, and liver. Here we show that the PPARδ agonist KD3010, but not the well-validated GW501516, dramatically ameliorates liver injury induced by carbon tetrachloride (CCl_4) injections. Deposition of extracellular matrix proteins was lower in the KD3010-treated group than in the vehicle- or GW501516-treated group. Interestingly, profibrogenic connective tissue growth factor was induced significantly by GW501516, but not by KD3010, following CCl_4 treatment. The hepatoprotective and antifibrotic effect of KD3010 was confirmed in a model of cholestasis-induced liver injury and fibrosis using bile duct ligation for 3 wk. Primary hepatocytes treated with KD3010 but not GW501516 were protected from starvation or CCl_4-induced cell death, in part because of reduced reactive oxygen species production. In conclusion, our data demonstrate that an orally active PPARδ agonist has hepatoprotective and antifibrotic effects in animal models of liver fibrosis, suggesting a possible mechanistic and therapeutic approach in treating patients with chronic liver diseases.

hepatic stellate cells Kupffer cells liver cirrhosis

Liver fibrosis is a common consequence of chronic liver injury including alcohol abuse, viral hepatitis, autoimmune disease, and nonalcoholic steatohepatitis. Chronic liver disease can progress to cirrhosis and hepatocellular carcinoma. Cirrhosis is a major health burden worldwide and currently is the 12th leading cause of death in the United States. Liver fibrosis is reversible if the causative agent (e.g., alcohol consumption, hepatitis B and C viral infections, or biliary obstruction) is removed successfully (1). However, the underlying causative agent is treated successfully only in subsets of patients with liver diseases, and there are no specific treatments for liver fibrosis. An ideal antifibrotic therapy would be liver specific, well tolerated when administered for prolonged periods of time, and effective in attenuating excessive collagen deposition without affecting normal extracellular matrix synthesis (2).

Peroxisome proliferator-activated receptors (PPARs) are members of the nuclear receptor family of ligand-activated transcription factors. They form heterodimers with retinoid X receptor (RXR) and bind to consensus DNA sites. Ligand binding induces a conformational change in PPAR–RXR complexes, releasing repressors in exchange for coactivators, and results in modulation of gene transcription. PPARs are able to transrepress as well as transactivate genes (3). Functional dissection of ligand-dependent coregulators of PPARs reveals that their transcriptional regulation is linked to histone modification and chromatin remodeling. All three subtypes of PPARs, including PPARδ, can be activated by fatty acids and fatty-acid derivatives. Based on studies using gene deletion and synthetic agonists, PPARδ is emerging as a key metabolic regulator. PPARδ agonists improve glucose and lipid homeostasis (4, 5) and increase skeletal muscle fatty-acid metabolism. PPARδ agonists have been shown to be exercise mimetics and to increase endurance in mice that already are undergoing exercise (6). PPARδ has anti-inflammatory activities, including inhibition of cytokine production and promoting the alternative activation of macrophages (7).

To determine whether PPARδ agonists are beneficial in experimental liver fibrosis, mice were treated orally with a PPARδ agonist, KD3010, or with the well-validated PPARδ agonist GW501516. Unexpectedly, KD3010, but not GW501516, showed hepatoprotective and antifibrotic effects in liver fibrosis induced by carbon tetrachloride (CCl_4) or bile duct ligation (BDL).

Results

PPARδ Agonist KD3010 Protects from Liver Injury. Liver injury was induced by repeated injections of CCl_4, and mice were treated daily with vehicle, the widely used PPARδ agonist GW501516 (6), or the PPARδ agonist KD3010 by oral gavage. Control oil-injected mice did not show any liver damage (Fig. 1*A*). Liver injury consisting of hepatocyte death and inflammation was seen in the vehicle- or GW501516-treated group injected with CCl_4 on H&E-stained liver sections but was markedly reduced in the KD3010-treated group (Fig. 1*A*). This result was confirmed by [redacted]e (ALT) levels, which were reduced only in the KD3010 group compared with other groups (Fig. 1*B*). Both KD3010 and GW501516 induced PPARδ-responsive genes such as adipose differentiation-related protein (*ADFP*) and uncoupling protein 2 (*UCP2*), but not PPARα- and PPARγ-specific responsive genes such as *FGF21* and *CD36*, respectively (Fig. 1*C*).

KD3010-Treated Mice Show Less Hepatic Fibrosis. Fibrillar collagen deposition as a measure of liver fibrosis was determined by Sirius Red staining. Vehicle- or GW501516-treated animals showed bridging fibrosis. Fibrosis was lower in the KD3010 group (Fig. 1*D*) than in the other groups. The lower level of Sirius Red staining was confirmed by morphometric analysis (Fig. 1*E*). Hydroxyproline content, a measure for total collagen, was reduced in the KD3010 group (Fig. 1*F*). Mice subjected to CCl_4 and treated with KD3010 showed control levels of the inflammatory cytokine *TNFα* compared with the vehicle- and GW501516-treated groups (Fig. 1*G*). Similarly, α-smooth muscle actin (*αSMA*) mRNA, a marker of hepatic stellate cell activation, also was down-regulated in the KD3010 group. An

Author contributions: K.I., C.S., R.T.Y., M.D., R.M.E., D.A.B., and B.S. designed research; K.I., M.H., Y.-H.P., K.T., Y.K., and E.Y. performed research; K.I., C.S., R.T.Y., M.D., R.M.E., D.A.B., and B.S. analyzed data; and K.I., D.A.B., and B.S. wrote the paper.

The authors declare no conflict of interest.

Data deposition: The microarray data reported in this paper have been deposited in the Gene Expression Omnibus (GEO) database (accession code GSE32121).

[1]To whom correspondence may be addressed. E-mail: evans@salk.edu or beschnabl@ucsd.edu.

See Author Summary on page 7965 (volume 109, number 21).

This article contains supporting information online at www.pnas.org/lookup/suppl/doi:10.1073/pnas.1202464109/-/DCSupplemental.

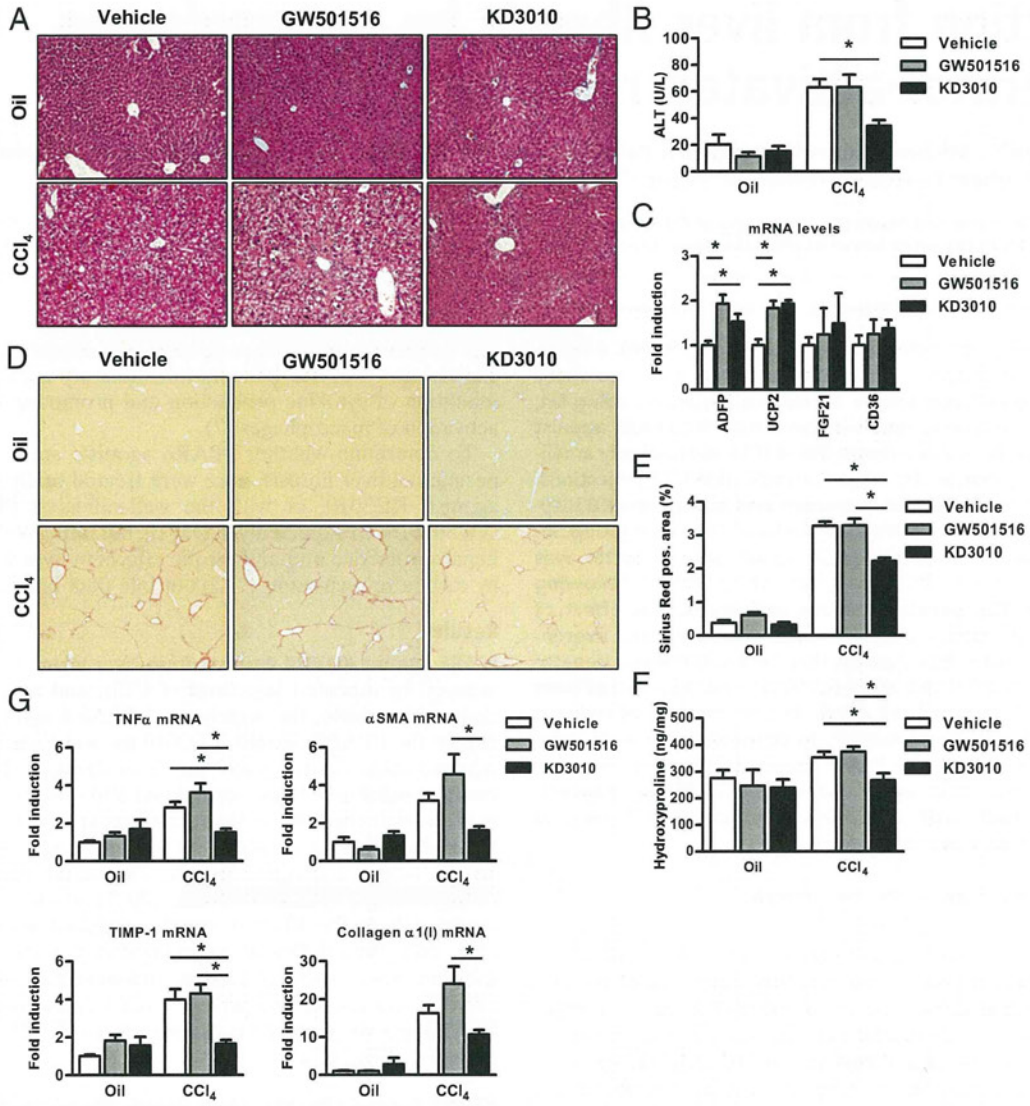

Fig. 1. Reduced liver injury and hepatic fibrosis in mice treated with the PPARδ agonist KD3010. Mice were injected i.p. 12 times with oil as control ($n = 4$ in each group) or with CCl_4 and were administered vehicle ($n = 14$), GW501516 (2 mg/kg; $n = 12$), or KD3010 (10 mg/kg; $n = 11$) daily by oral gavage. (*A*) Representative H&E-stained liver sections are shown. (*B*) ALT levels were measured in the serum of mice. (*C*) Relative gene-expression levels of *ADFP*, *UCP2*, *FGF21*, and *CD36* were determined in the liver of mice treated with vehicle, GW501516, or KD3010 for 5 wk ($n = 4$ in each group). (*D* and *E*) Collagen deposition was evaluated by Sirius Red staining and quantitated by image analysis. Representative sections stained with Sirius Red are shown for vehicle-, GW501516-, and KD3010-treated mice. (*F*) Hydroxyproline content was measured in the liver of mice. (*G*) Hepatic *TNFα*, *αSMA*, *TIMP-1*, or *collagen α1(I)* gene expression was assessed by qPCR. $^*P < 0.05$.

equally impressive reduction of hepatic expression of mRNA encoding *collagen α1(I)* was found in the KD3010 group, and induction of tissue inhibitor of matrix metalloproteinases (*TIMP*)-*1*, an important mediator of liver fibrosis, was decreased in the KD3010 group (Fig. 1*G*). Taken together, PPARδ ligand activation by KD3010, but not by GW501516, protects against chemically induced liver injury and fibrosis and reduces hepatic inflammation.

KD3010 Protects Against Cholestasis-Induced Liver Fibrosis. To determine whether the PPARδ agonist KD3010 suppresses hepatic fibrosis induced by a different etiology, mice underwent cholestatic liver injury by BDL and were treated daily with vehicle or KD3010. Twenty-one days after BDL, liver injury was reduced markedly in the KD3010 group as seen on H&E-stained liver sections (Fig. 2*A*). Mice treated with KD3010 showed a significant reduction in fibrosis as evidenced by Sirius Red staining (Fig. 2 *B* and *C*). The survival rate was significantly higher in PPARδ agonist-treated mice subjected to BDL (Fig. 2*D*). In addition, compared with mice treated with vehicle, the KD3010 BDL group showed decreased expression of inflammatory genes in the liver, including *TNFα* and *IL-1β* (Fig. 2*E*). Consistent with the histopathology, hepatic *TIMP-1* and collagen α1(I) gene expression was decreased following PPARδ ligand activation (Fig. 2*E*). Thus, PPARδ activation protects from both hepatotoxic and cholestatic liver fibrosis.

Cellular Expression of PPARδ in the Liver. To determine which hepatic cells express PPARδ in vivo, we performed double staining for PPARδ and F4/80, as a marker for Kupffer cells, or desmin, as a marker for hepatic stellate cells. PPARδ protein expression was found in the nucleus of Kupffer cells and hepatic stellate cells (Fig. 3*A*). Notably, not all Kupffer cells or hepatic stellate cells expressed PPARδ, consistent with reports of heterogeneous

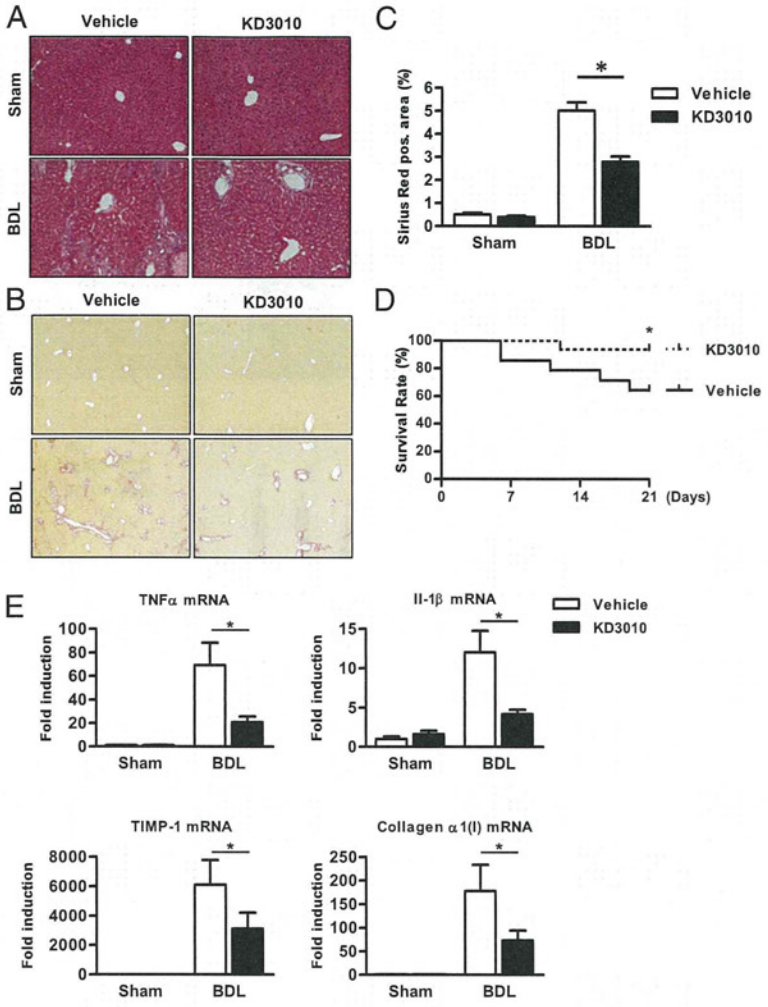

Fig. 2. Mice receiving KD3010 are protected from liver fibrosis after BDL. Mice underwent sham operation ($n = 4$ in each group) or BDL for 21 d and were treated with vehicle ($n = 9$) or KD3010 ($n = 14$). (*A*) Representative H&E-stained liver sections are shown. (*B* and *C*) Hepatic fibrosis was assessed by Sirius Red staining. Representative sections are shown. (*D*) Survival of mice receiving vehicle ($n = 14$) or KD3010 ($n = 16$) following BDL for 21 d. (*E*) Hepatic *TNFα*, *IL-1β*, *TIMP-1*, or *collagen α1(I)* gene expression was assessed by qPCR. $^*P < 0.05$.

Kupffer cell and hepatic stellate cell populations (8). Hepatocytes showed weak positive staining for PPARδ protein. Adipose tissue was used as a positive staining control (Fig. S1).

A similar expression pattern was observed on the gene level. *PPARδ* mRNA was expressed predominantly in Kupffer cells and in hepatic stellate cells isolated from normal liver but was expressed only minimally in hepatocytes (Fig. 3*B*). To confirm the responsiveness of hepatocytes to a PPARδ ligand, hepatocytes were isolated, and expression of PPARδ-responsive genes was determined following treatment with KD3010. KD3010 induced PPARδ-responsive genes such as *ADFP*, pyruvate dehydrogenase kinase, isoenzyme 4 (*PDK4*), and angiopoietin-like 4 (*Angptl4*) but not the PPARα- and PPARγ-responsive genes, *FGF21* and *CD36*, respectively (Fig. 3*C*). These results indicate that KD3010 is capable of activating PPARδ in hepatocytes.

Polarization State of Kupffer Cells Is Not Affected by KD3010. In response to different stimuli, Kupffer cells are capable of differentiating into two polarization states, M1 and M2. LPS promotes Kupffer cell differentiation to a classical, M1 phenotype. The M1 activation pattern is responsible for up-regulating proinflammatory mediators (9). To delineate the effects of KD3010 on Kupffer cells, primary Kupffer cells were isolated from wild-type mice and cultured in the presence of KD3010. The morphology did not change following treatment with KD3010 for 1 d in culture compared with vehicle-treated cells (Fig. S2*A*). KD3010 induced PPARδ-responsive genes such as *ADFP*, *PDK4*, and *Angptl4* in primary Kupffer cells (Fig. 3*D*). LPS-induced expression of *TNFα*, *IL-6*, and *IL-1β* was not suppressed by KD3010 in cultured Kupffer cells (Fig. S2*B*). In contrast, an alternative or M2 phenotype of Kupffer cells is induced in response to IL-4 and IL-13. The M2 phenotype is thought to produce anti-inflammatory factors and to promote tissue repair after inflammation and/or injury (7, 10). IL-4–induced expression of M2 markers such as *arginase1* and macrophage galactose-type C-type lectin 1 (*Mgl-1*) was not affected following KD3010 treatment in cultured Kupffer cells (Fig. S2*B*). Thus, KD3010 induces a common set of PPARδ target genes such as *ADFP*, *PDK4*, and *Angptl4* in both M1 and M2 Kupffer cells.

PPARδ Ligand KD3010 Does Not Decrease the Activation and Fibrogenic Potential of Hepatic Stellate Cells. To explain the beneficial effect of KD3010 in liver fibrosis, we next focused on hepatic stellate cells. Hepatic stellate cells isolated from wild-type mice did not change their morphology following treatment with

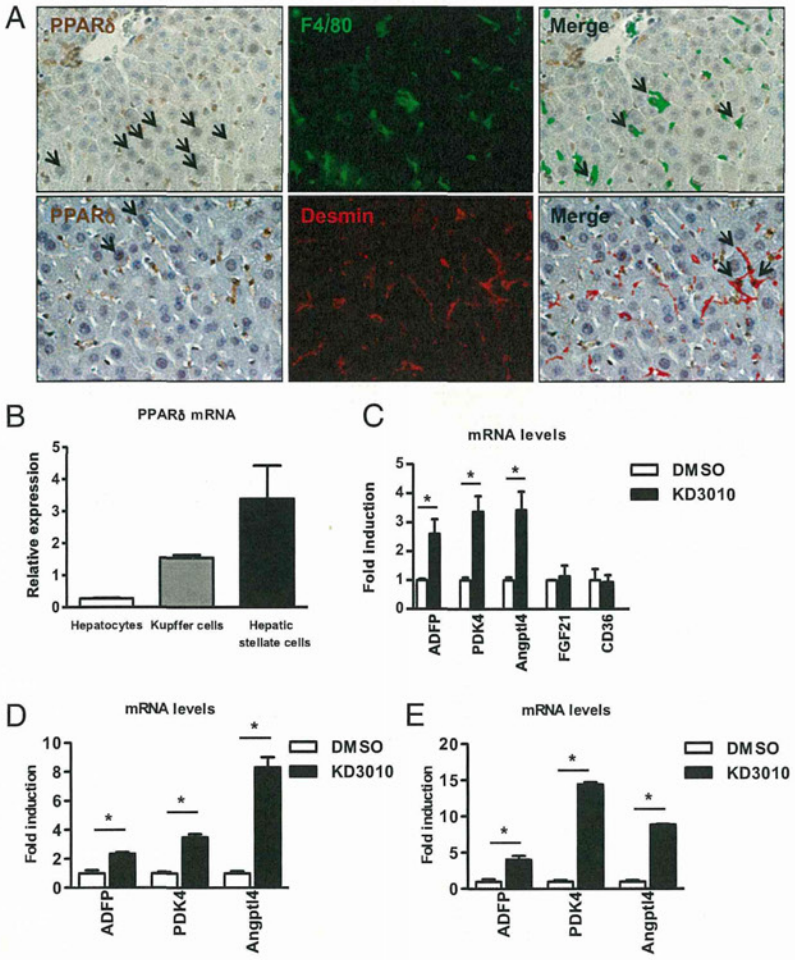

Fig. 3. Hepatocytes express PPARδ. (*A*) Immunohistochemical staining for PPARδ (brown), and immunofluorescent staining for F4/80 (green) and desmin (red) was performed to detect PPARδ protein in Kupffer cells and hepatic stellate cells, respectively. Black arrows indicate positively stained hepatocytes (*Left*), double-positive Kupffer cells (*Upper Right*), and hepatic stellate cells (*Lower Right*). (*B*) Liver cell fractions were isolated from a normal liver. PPARδ mRNA was analyzed by qPCR and normalized to 18S. The mean of three independent isolations is shown. (*C*) Hepatocytes were cultured with DMSO or KD3010 (5 μM). Gene expression of *ADFP*, pyruvate dehydrogenase kinase, isoenzyme 4 (*PDK4*), angiopoietin-like 4 (*Angptl4*), fibroblast growth factor (*FGF*)-*21*, and *CD36* was analyzed by qPCR and normalized to 18S. The mean of four independent experiments are shown. (*D*) Kupffer cells were cultured with DMSO or KD3010 (1 μM). Gene expression of *ADFP*, *PDK4*, and *Angptl4* was analyzed by qPCR and normalized to 18S. (*E*) Hepatic stellate cells were cultured with DMSO or KD3010 (1 μM). Gene expression of *ADFP*, *PDK4*, and *Angptl4* was analyzed by qPCR and normalized to 18S. **P* < 0.05.

KD3010 for 3 d in culture compared with vehicle-treated cells (Fig. S3*A*). Although KD3010 induced PPARδ-responsive genes such as *ADFP*, *PDK4*, and *Angptl4* (Fig. 3*E*), hepatic stellate cells incubated with KD3010 showed no change in the expression of fibrogenic genes *αSMA*, *TIMP-1*, and *collagen α1(I)* or the proliferation marker *cyclin D1* (Fig. S3*B*). *Hepatocyte growth factor* (*HGF*) was induced in KD3010-treated hepatic stellate cells compared with control cells (Fig. S3*B*). Thus, KD3010 does not modulate fibrogenic properties of hepatic stellate cells.

PPARδ Ligand Activation Protects Hepatocytes from Starvation and CCl_4-Induced Cell Death. We then focused on hepatocytes as potential targets for the beneficial effect of KD3010 in liver injury and fibrosis. KD3010 protected cultured hepatocytes from starvation-induced cytotoxicity, as evidenced by reduced ALT in the supernatant and reduced cell death (released LDH) (Fig. 4 *A*–*C*). In addition, KD3010 protected cultured hepatocytes from CCl_4-induced cell death, as assessed by diminished propidium iodide (PI) staining (Fig. 4*D*), and reduced ALT levels in the supernatant (Fig. 4*E*). The hepatoprotective effect of KD3010 was absent in PPARδ-deficient hepatocytes (Fig. 4*E*), demonstrating that the hepatoprotection of KD3010 is not an off-target effect.

Because reduced oxidative stress might mediate the protection from cell death, reactive oxygen species (ROS) were measured and indeed were lower in CCl_4-treated hepatocytes incubated with KD3010, whereas hepatocytes incubated with GW501516 showed more ROS production (Fig. 4*F*). KD3010 treatment of wild-type hepatocytes decreased thiobarbituric acid-reactive substances (TBARS), a measure of lipid peroxidation, after CCl_4 exposure, but this effect was not seen in PPARδ-deficient hepatocytes (Fig. 4*G*). We next examined cytochrome P450 (Cyp) expression, because its function is to catalyze the oxidation of organic substances. Gene expression of several Cyp family members was induced following incubation with KD3010. However, *Cyp2E1*, the CCl_4-metabolizing enzyme, was not affected by KD3010 (Fig. 4*H*). Thus, KD3010 induces Cyp family members, decreases ROS in hepatocytes, and protects hepatocytes from starvation and toxic cell death.

To explain further the differences between KD3010 and GW501516, we compared the gene-activation profile of the two compounds in cultured hepatocytes by gene-expression micro-

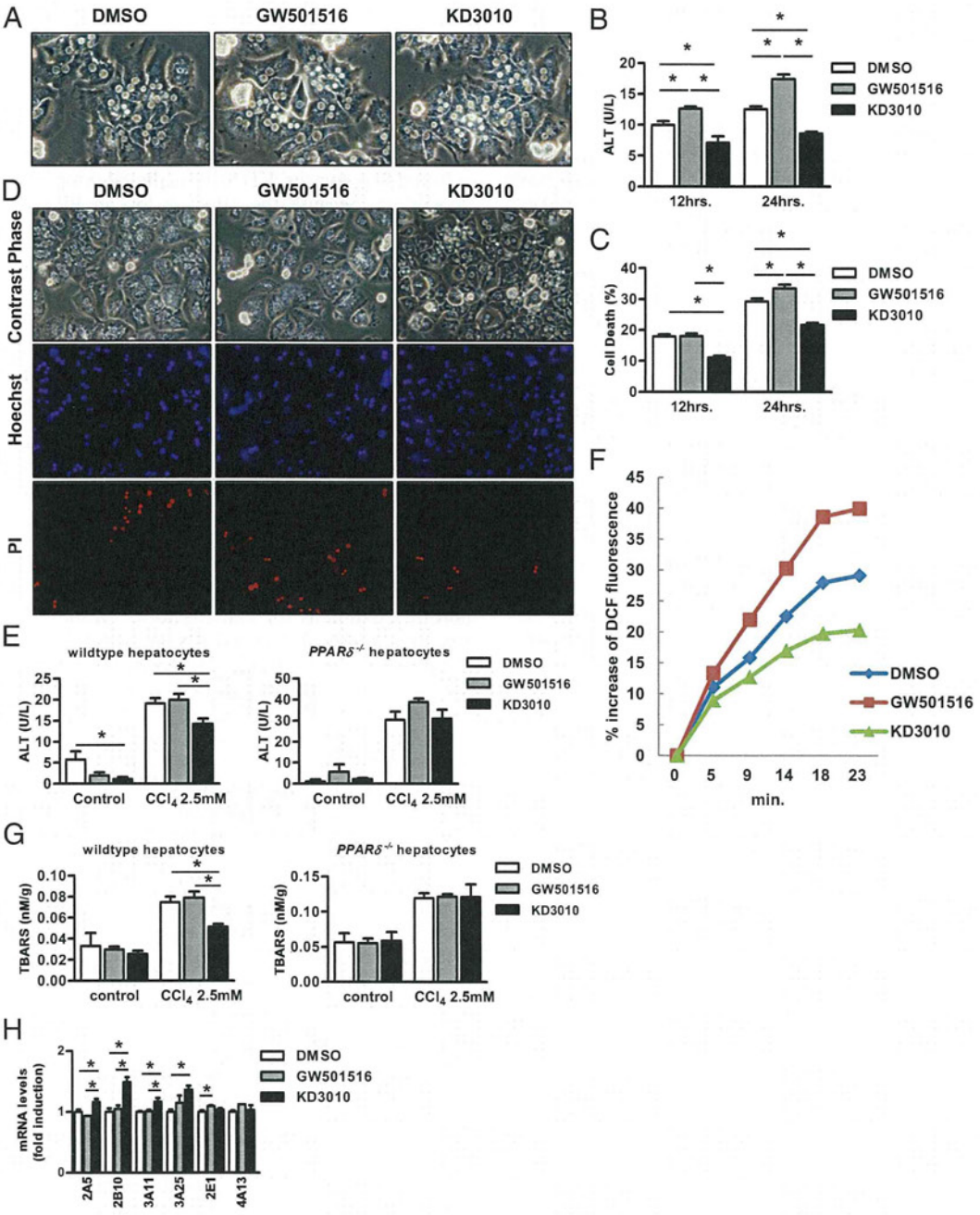

Fig. 4. KD3010 protects hepatocytes from cell death in culture. Hepatocytes were cultured in KRB without glucose and without FCS for indicated time periods in the presence of DMSO, GW501516 (100 nM), or KD3010 (5 μM). (*A*) Representative photomicrographs are shown. ALT was measured in the supernatant of cells (*B*), and cell death was assessed (*C*). (*D*) CCl_4 (2.5 mM) was added to hepatocytes after 12 h in the presence of DMSO, GW501516 (100nM) or KD3010 (5 μM). Representative photomicrographs of cells and Hoechst- and PI-stained hepatocytes are shown. (*E*) CCl_4-induced cell death was assessed in wild-type and PPARδ-deficient hepatocytes by measuring ALT in the supernatant. (*F*) Hepatocytes cultured with DMSO, GW501516 (100 nM), or KD3010 (5 μM) for 12 h were loaded with redox-sensitive dye CM-H_2DCFDA (10 μM) for 20 min. Fluorescent signals were quantified continuously for 23 min using a fluorometer. (*G*) TBARS were assessed in wild-type and PPARδ-deficient hepatocytes. (*H*) Hepatocytes were cultured in KRB in the presence of DMSO, GW501516 (100 nM) or KD3010 (5 μM) for 12 h. qRT-PCR was performed for Cyp family members. Results shown are the mean of four different hepatocyte isolations.*$P < 0.05$.

array analysis. Surprisingly, the two PPARδ agonists had distinct gene-expression profiles (Fig. S4 *A–C* and Tables S1 and S2). Known PPARδ-responsive genes such as *PDK4* and carnitine palmitoyltransferase 2 were induced by both agonists. KD3010 caused a larger change in gene expression than did GW501516. Interestingly, connective tissue growth factor (*CTGF*) was induced by GW501516 but not by KD3010. We therefore compared hepatic *CTGF* gene expression following CCl_4 treatment in mice gavaged with GW501516 or KD3010. Similar to the in vitro results, *CTGF* mRNA was significantly higher in GW501516-treated than in vehicle-treated mice, but there was no difference between KD3010- and vehicle-treated mice following repeated CCl_4 injections (Fig. S4*D*). CTGF has potent profibrogenic properties and is produced and secreted by hepatocytes (11). Recently CTGF has been shown to be induced by p53 in hepatocytes and to result in liver fibrosis (12), possibly

thereby contributing to the different effects on liver fibrosis observed with GW501516 and KD3010.

Discussion

To address the effect of PPARδ activation on chronic liver diseases, we took an unbiased approach to test a potent and highly selective PPARδ agonist, KD3010, in mouse models of liver fibrosis induced by hepatotoxicity (CCl_4 injections) and cholestasis (BDL). KD3010 shows dramatic antifibrotic effects in vivo and was more effective than the well-validated PPARδ agonist GW501516. Hepatocytes appear to be the target for PPARδ ligand activation, because KD3010 protects cultured hepatocytes from starvation- and CCl_4-induced cell death. Thus, a hepatoprotective effect upon ligand activation mediates the beneficial effect of KD3010 in experimental animal models of liver fibrosis.

The role of PPRAδ in chronic liver disease has not been examined previously. PPARδ deficiency increases acute liver toxicity induced by azoxymethane or CCl_4 in mice (13), whereas treatment with the PPARδ ligand GW0742 ameliorates acute CCl_4-induced liver toxicity in a PPARδ-dependent fashion (14). The cellular mechanism was not identified in these studies (13). In contrast to the beneficial effect of PPARδ ligand activation in acute liver disease, enhanced acute liver toxicity after one dose of CCl_4 was reported to occur in rats when another PPARδ ligand, L165041, was administered concomitantly (15). Our study demonstrates that a highly specific PPARδ agonist, KD3010, showed potent beneficial effects in two models of liver injury and fibrosis, whereas the known PPARδ agonist GW501516 did not affect chronic liver injury. Consistent with our results, GW501516 did not affect liver fibrosis in a choline-deficient, ethionine-supplemented mouse model of steatohepatitis (16). Differences in the physiological outcomes of specifically targeted nuclear receptor pharmacophores are well documented in the steroid receptor family for estrogens, glucocorticoids, and androgens. In addition, differential outcomes have been reported recently for targeted synthetic farnesoid X receptor ligands, as demonstrated by global gene-expression profiles (17). The differences reported here for the PPARδ agonists can be attributed to a number of different factors, including different specificities for other PPAR isoforms, potencies of different synthetic compounds, and in vivo pharmacological properties of the compounds including differential tissue distribution, degradation, and clearance. This study demonstrates that distinct structural pharmacophores, although classified as agonists, can confer widely differing benefits in the pathological setting when studying the effects of nuclear receptor-targeted agonists.

PPARδ plays an important role in energy, glucose, and lipid homeostasis. This role may be mediated in part by alternative M2 activation of macrophages/Kupffer cells. Genetic ablation of PPARδ in bone marrow cells impairs alternative activation of tissue macrophages and predisposes mice to the development of insulin resistance and metabolic syndrome, including adiposity and hepatic steatosis on a high-fat diet (7). PPARδ is induced by T-helper type 2 cytokines derived from hepatocytes or adipocytes to induce alternative activation of adipose tissue macrophages or Kupffer cells, suggesting that M2 macrophages have a profound influence on oxidative metabolism and lipid homeostasis. Alternatively activated macrophages attenuate inflammation in the liver and also in white fat tissue (7, 10). In contrast, recent studies do not support a role for alternative activation of macrophages mediated by PPARδ. Loss of PPARδ in bone marrow-derived cells did not affect glucose tolerance in mice fed a high-fat diet (18). PPARγ, but not PPARδ, activation promotes human monocyte differentiation toward alternative macrophages (19). Although Kupffer cells express endogenous PPARδ, our study provides evidence that Kupffer cells are not an important target for PPARδ ligand activation to mediate its antifibrotic effect. KD3010 did not modulate in vitro activation and the polarization state of Kupffer cells. Hepatic stellate cells, the main cell type producing extracellular matrix in liver fibrosis, express endogenous PPARδ, but their fibrogenic properties are not changed following PPARδ activation in vitro.

Hepatocytes, the predominant liver cell type, express PPARδ and induce PPARδ-responsive genes upon KD3010 treatment. KD3010, but not GW501516, protects cultured hepatocytes from starvation- and CCl_4-induced cell death. In fact, GW501516 increased ROS production and starvation-induced cell death in cultured hepatocytes. KD3010-mediated cytoprotection is PPARδ dependent, because the effect is lost in PPARδ-deficient hepatocytes. The mechanism likely involves expression of Cyp enzymes, which are stimulated by KD3010 and result in oxidation and detoxification of organic substances, whereas GW501516 did not alter expression of Cyp enzymes. In addition to the PPARδ-dependent cytoprotective effect, we also demonstrate the induction of CTGF by GW501516, which is a strong profibrotic cytokine. Combined, the cytoprotection and the absence of a profibrogenic cytokine confer protection against fibrosis and explain the differences between KD3010 and GW501516 observed in our study. Our study identifies hepatocytes as the main target cell population in the liver that mediates the beneficial effect of KD3010 in a PPARδ-dependent fashion.

Chronic liver disease results in hepatic fibrosis. The only current treatment paradigm for patients with hepatic fibrosis is treatment of the underlying liver disease (20). If the causative agent cannot be removed, there are currently no effective antifibrotic treatments for patients with chronic liver diseases (21). Experimental studies in rodents have revealed targets to prevent the progression of fibrosis. However, the efficacy of most treatments has not been tested in humans. Additionally, promising targets identified in rodents may result in undesirable side effects in humans. For example, inhibition of the profibrotic cytokine TGFβ-1 may favor cancer development, especially in liver cirrhosis, which is a premalignant state (2). On the other hand, PPARδ deficiency results in azoxymethane-induced regenerative liver cell hyperplasia, suggesting that PPARδ protects against enhanced cell proliferation in the liver (13). Insights into the mechanisms of the development of hepatic fibrosis provide an opportunity to develop therapeutic interventions for human clinical use. A PPARδ agonist may serve as a treatment option for liver fibrosis. The findings reported here should promote further clinical investigation into the potential use of a PPARδ agonist in treating patients with chronic liver diseases.

Materials and Methods

Mouse Models of Liver Fibrosis. Male 11-wk-old C57/B6 mice were treated with CCl_4 (2 μL/g body weight; 1:4 dilution with corn oil) or with corn oil as control (2 μL/g body weight) by i.p. injection every third day. Injections were repeated for a total of 12 times. Livers were harvested 3 d after the last injection. BDL or sham operation as control was performed as described previously (22), and livers were harvested 21 d later. All animal procedures were performed under the guidelines set by The University of California, San Diego Institutional Animal Care and Use Committee and are in accordance with those set by the National Institutes of Health.

Treatment Protocol. KD3010 (chemical name (S)-4-[cis-2,6-dimethyl-4-(4-trifluoromethoxy-phenyl)piperazine-1-sulfonyl]-indan-2-carboxylic acid tosylate) (Fig. S5) is a potent, orally active, and selective PPARδ agonist (Kalypsys Inc.). Phase I clinical trials have successfully been completed in healthy volunteers and demonstrated safety and tolerability without clinically relevant treatment- or dose-related trends in the laboratory, vital sign, ECG, or physical examination safety parameters (www.kalypsys.com). KD3010 has no appreciable interaction with human, rhesus, or murine PPARα and PPARγ receptors, as evidenced by EC_{50} values in excess of 7–10 μM. Cell-based reporter gene assays indicate that KD3010 (up to 10 μM) does not affect the function of mouse/human pregnane X receptor and human constitutive androstane receptor. For in vitro experiments we used concentrations of 1–5 μM. Mean plasma compound concentration of mice treated with CCl_4 and gavaged with KD3010 was 4 ± 0.8 μM (at time of harvesting). Mice were assigned randomly into groups at the beginning of the study. The study was conducted in a blinded fashion, and the researchers performing the in vivo

experiments (CCl_4 treatment and BDL; Figs. 1 and 2) remained blinded to the nature of the experimental drugs until all data were analyzed. Mice were treated daily with vehicle or KD3010 (10 mg/kg) by oral gavage. At times of CCl_4 injections, the compounds were administered 2 h after the last gavage was given. Similarly, a well-characterized PPARδ agonist GW501516 (2 mg/kg) or vehicle was administered to mice daily by gavage (6).

Liver Enzymes and Staining Procedures. Blood was taken at the time of harvesting. ALT in the plasma was measured by the Infinity kit (Thermo Fisher Scientific) according to the manufacturer's instructions. Formalin-fixed liver samples were embedded in paraffin and stained with H&E. Sirius Red staining [saturated picric acid containing 0.1% (wt/vol) Direct Red 80] was performed as described (22). The Sirius Red-positive area was measured at a final magnification of 40×. The entire median lobe of the liver was imaged, and 6–14 images per animal were taken and analyzed using National Institutes of Health Image J. The results are presented as percentage area positively stained for Sirius Red. Immunohistochemistry and immunofluorescence were performed using anti-PPARδ antibody (1:100; Santa Cruz), anti-desmin antibody (1:200; DAKO), and anti-F4/80 antibody (1:200; eBioscience) as described (22).

Hydroxyproline Measurement. Liver tissue was homogenized in ice-cold distilled water (900 μL) using a Power Gen homogenizer (Fisher). Subsequently, 125 μL of 50% (wt/vol) trichloroacetic acid was added, and the homogenates were incubated further on ice for 20 min. Precipitated pellets were hydrolyzed for 18 h at 110 °C in 6N HCL. After hydrolysis, the samples were filtered and neutralized with 10N NaOH, and the hydrolysates were oxidized with Chloramine-T (Sigma) for 25 min at room temperature. The reaction mixture then was incubated in Ehrlich's perchloric acid solution at 65 °C for 20 min and cooled to room temperature. Sample absorbance was measured at 560 nm in duplicate. Purified hydroxyproline (Sigma) was used to set a standard. Hydroxyproline content was expressed as nanogram of hydroxyproline per milligram liver.

Gene-Expression Analysis. Total RNA was extracted with TRIZOL (Invitrogen). RNA was digested with DNase using the DNA-free kit (Ambion). DNase-treated RNA was reverse transcribed using the High Capacity cDNA Reverse Transcription kit (ABI). Real-time quantitative PCR (qPCR) was performed for 40 cycles of 15 s at 95 °C and 60 s at 60 °C using an ABI 7000 sequence detection system. The relative abundance of the target genes was obtained by calculating against a standard curve and normalized to 18S or cyclophilin as internal control. Probes purchased from ABI or primers from the National Institutes of Health mouse qprimer depot were used with SYBR green (Bio-Rad). Microarrays were performed as described (6). Briefly, samples were labeled and hybridized to Affymetrix Mouse Genome 430 2.0 arrays ($n = 3$ in each group). Microarray data have been deposited in the Gene Expression Omnibus (accession code GSE32121). Microarray data analysis was performed as described (23). In brief, image data were converted into nonnormalized sample probe profiles using the BeadStudio software (Illumina) and analyzed on the VAMPIRE microarray analysis framework48. We constructed stable variance models for each of the two experimental conditions and identified differentially expressed probes using the unpaired VAMPIRE significance test with a two-sided, Bonferroni-corrected threshold (α_{Bonf}) of 0.05. The VAMPIRE statistical test is a Bayesian statistical method that computes a model-based estimate of noise at each level of gene expression. This estimate then was used to assess the statistical significance of the apparent differences in gene expression in the two experimental conditions.

Isolation and Culture of Hepatocytes, Kupffer Cells, and Hepatic Stellate Cells. Isolation of liver-cell fractions from normal liver using magnetic cell sorting (MACS) has been described (22). Kupffer cells and hepatic stellate cells were isolated from mice by two-step collagenase–pronase perfusion followed by three-layer discontinuous density gradient centrifugation with 8.2% (wt/vol) and 14.5% (wt/vol) Nycodenz (Accurate Chemical and Scientific Corporation) to obtain Kupffer-cell and hepatic stellate-cell fractions. Hepatic stellate cells were collected between the 0 and 8.2% (wt/vol) layer. The Kupffer-cell fraction was selected negatively by MACS using anti-LSEC Micro Beads (Miltenyi Biotech). Kupffer cells were cultured with DMSO or KD3010 (1 μM) for 1 d before stimulation by LPS (1 ng/mL for 4 h) or IL-4 (10 ng/mL for 24 h). Hepatic stellate cells were cultured with DMSO or KD3010 (5μM) for 3 d before harvesting. To induce starvation-associated cell death, hepatocytes were cultured in Waymouth's medium containing 10% (vol/vol) FCS for 3.5 h; Waymouth's medium then was changed to Krebs–Ringer buffer without glucose (KRB) in the presence of DMSO, KD3010 (5 μM), or GW501516 (100 nM). In some experiments, CCl_4 (2.5 mM) was added to hepatocytes after 12 h. Cell death was assessed by measuring ALT in the supernatant, by using a Cytotoxicity Detection Kit (Roche), or by staining with PI. Hepatocytes were isolated from wild-type or PPARδ-deficient mice (4) and were cultured in 96-well black-bottomed plates in KRB for 12 h in the presence of DMSO, KD3010 (5 μM), or GW501516 (100 nM). Cells were loaded with the redox-sensitive dye CM-H_2DCFDA (10 μM) diluted in KRB for 20 min at 37 °C. Cells then were rinsed twice with KRB and stimulated with CCl_4 (2.5 mM). CM-H_2DCFDA fluorescence was detected at excitation and emission wavelengths of 488 nm and 520 nm, respectively. ROS formation was measured in a time course of 23 min using a multiwell fluorescence scanner (Fluostar Optima; BMG Labtech). TBARS were measured by using OxiSelect TBARS Assay Kit (MDA Quantitation). For microarray analysis, RNA was extracted from hepatocytes cultured in Waymouth's medium containing 10% (vol/vol) FCS in the presence of DMSO, KD3010 (5 mM), or GW501516 (100 nM) for 12 h.

Statistical Analysis. Results are reported as mean ± SEM, unless otherwise stated. Comparisons among multiple groups were performed by one-way ANOVA with post hoc test (Tukey's Multiple Comparison Test). Mouse survival data were analyzed statistically by using the Log-rank (Mantel–Cox) test. Comparisons between two groups were performed by the Mann–Whitney *u*-statistic test. $P < 0.05$ was considered statistically significant. All statistical analyses were performed using GraphPad Prism.

ACKNOWLEDGMENTS. KD3010 was provided as a gift from Kalypsys, Inc. This study was supported in part by National Institutes of Health Grants K08 DK081830 and R01 AA020703 (to B.S.), R01 DK072237 (to D.A.B.), R01 DK057978 (to R.M.E.), and R24 DK090962 (to D.A.B. and R.M.E.). This study also was supported by University of California, San Diego Digestive Diseases Research Development Center Grant DK080506 (to B.S.) and by Award K12-HD000850 from the Eunice Kennedy Shriver National Institute of Child Health and Human Development (to E.Y.). R.M.E. was supported by the Helmsley Charitable Trust and by the Howard Hughes Medical Institute. R.M.E. is an investigator of the Howard Hughes Medical Institute and March of Dimes Chair in Molecular and Developmental Biology at the Salk Institute. E.Y. is a Fellow of the Pediatric Scientist Development Program.

1. Bataller R, Brenner DA (2005) Liver fibrosis. *J Clin Invest* 115:209–218.
2. Schnabl B, Scholten D, Brenner DA (2008) What is the potential role of antifibrotic agents for the treatment of liver disease? *Nat Clin Pract Gastroenterol Hepatol* 5: 496–497.
3. Barish GD, Narkar VA, Evans RM (2006) PPAR delta: A dagger in the heart of the metabolic syndrome. *J Clin Invest* 116:590–597.
4. Lee CH, et al. (2006) PPARdelta regulates glucose metabolism and insulin sensitivity. *Proc Natl Acad Sci USA* 103:3444–3449.
5. Oliver WR, Jr., et al. (2001) A selective peroxisome proliferator-activated receptor delta agonist promotes reverse cholesterol transport. *Proc Natl Acad Sci USA* 98: 5306–5311.
6. Narkar VA, et al. (2008) AMPK and PPARdelta agonists are exercise mimetics. *Cell* 134: 405–415.
7. Odegaard JI, et al. (2008) Alternative M2 activation of Kupffer cells by PPARdelta ameliorates obesity-induced insulin resistance. *Cell Metab* 7:496–507.
8. Magness ST, Bataller R, Yang L, Brenner DA (2004) A dual reporter gene transgenic mouse demonstrates heterogeneity in hepatic fibrogenic cell populations. *Hepatology* 40:1151–1159.
9. Olefsky JM, Glass CK (2010) Macrophages, inflammation, and insulin resistance. *Annu Rev Physiol* 72:219–246.
10. Kang K, et al. (2008) Adipocyte-derived Th2 cytokines and myeloid PPARdelta regulate macrophage polarization and insulin sensitivity. *Cell Metab* 7:485–495.
11. Gressner OA, Gressner AM (2008) Connective tissue growth factor: A fibrogenic master switch in fibrotic liver diseases. *Liver Int* 28:1065–1079.
12. Kodama T, et al. (2011) Increases in p53 expression induce CTGF synthesis by mouse and human hepatocytes and result in liver fibrosis in mice. *J Clin Invest* 121:3343–3356.
13. Shan W, et al. (2008) Peroxisome proliferator-activated receptor-beta/delta protects against chemically induced liver toxicity in mice. *Hepatology* 47:225–235.
14. Shan W, et al. (2008) Ligand activation of peroxisome proliferator-activated receptor beta/delta (PPARbeta/delta) attenuates carbon tetrachloride hepatotoxicity by downregulating proinflammatory gene expression. *Toxicol Sci* 105:418–428.
15. Hellemans K, et al. (2003) Peroxisome proliferator-activated receptor-beta signaling contributes to enhanced proliferation of hepatic stellate cells. *Gastroenterology* 124: 184–201.
16. Knight B, Yeap BB, Yeoh GC, Olynyk JK (2005) Inhibition of adult liver progenitor (oval) cell growth and viability by an agonist of the peroxisome proliferator activated receptor (PPAR) family member gamma, but not alpha or delta. *Carcinogenesis* 26: 1782–1792.
17. Downes M, et al. (2003) A chemical, genetic, and structural analysis of the nuclear bile acid receptor FXR. *Mol Cell* 11:1079–1092.

18. Marathe C, et al. (2009) Preserved glucose tolerance in high-fat-fed C57BL/6 mice transplanted with PPARgamma-/-, PPARdelta-/-, PPARgammadelta-/-, or LXRalphabeta-/- bone marrow. *J Lipid Res* 50:214–224.
19. Bouhlel MA, et al. (2009) Unlike PPARgamma, PPARalpha or PPARbeta/delta activation does not promote human monocyte differentiation toward alternative macrophages. *Biochem Biophys Res Commun* 386:459–462.
20. Poynard T, et al. (2002) Impact of pegylated interferon alfa-2b and ribavirin on liver fibrosis in patients with chronic hepatitis C. *Gastroenterology* 122:1303–1313.
21. Di Bisceglie AM, et al.; HALT-C Trial Investigators (2008) Prolonged therapy of advanced chronic hepatitis C with low-dose peginterferon. *N Engl J Med* 359: 2429–2441.
22. Taura K, et al. (2008) Hepatic stellate cells secrete angiopoietin 1 that induces angiogenesis in liver fibrosis. *Gastroenterology* 135:1729–1738.
23. Pei L, et al. (2011) Thyroid hormone receptor repression is linked to type I pneumocyte-associated respiratory distress syndrome. *Nat Med* 17:1466–1472.

Journal of Gastroenterology and Hepatology

JGHF

doi:10.1111/j.1440-1746.2011.07002.x

NOVEL INSIGHTS INTO LIVER AND PANCREATIC FIBROGENESIS

What's new in liver fibrosis? The origin of myofibroblasts in liver fibrosis

Keiko Iwaisako, David A Brenner and Tatiana Kisseleva

Department of Medicine, University of California, San Diego, La Jolla, California, USA

David A Brenner

Key words
hepatic stellate cell, liver fibrosis, myofibroblast, portal fibroblast.

Accepted for publication 11 November 2011.

Abstract

Chronic liver injury of many etiologies produces liver fibrosis and may eventually lead to the formation of cirrhosis. Fibrosis is part of a dynamic process associated with the continuous deposition and resorption of extracellular matrix, mainly fibrillar collagen. Studies of fibrogenesis conducted in many organs including the liver demonstrate that the primary source of the extracellular matrix in fibrosis is the myofibroblast. Hepatic myofibroblasts are not present in the normal liver but transdifferentiate from heterogeneous cell populations in response to a variety of fibrogenic stimuli. Debate still exists regarding the origin of hepatic myofibroblasts. It is considered that hepatic stellate cells and portal fibroblasts have fibrogenic potential and are the major origin of hepatic myofibroblasts. Depending on the primary site of injury the fibrosis may be present in the hepatic parenchyma as seen in chronic hepatitis or may be restricted to the portal areas as in most biliary diseases. It is suggested that hepatic injury of different etiology triggers the transdifferentiation to myofibroblasts from distinct cell populations. Here we discuss the origin and fate of myofibroblast in liver fibrosis.

Correspondence
Professor David A Brenner, Division of Gastroenterology, Department of Medicine, School of Medicine, University of California, San Diego, 9500 Gilman Drive #0602, Biomedical Sciences Building 1318, La Jolla, CA 92093-0602, USA. Email: dbrenner@ucsd.edu

Conflict of Interests: There are no conflicts of interests.

Introduction

Liver fibrosis results from continuous injury to the liver, including viral hepatitis, alcohol abuse, metabolic diseases, autoimmune diseases, and cholestatic liver diseases. In other words, fibrosis is a consequence of the excessive healing response triggered by chronic liver injury. The end stage of liver fibrosis, cirrhosis, is histologically characterized by increased deposition and altered composition of the extracellular matrix (ECM) and the appearance of regenerative nodules.[1] The destruction of the normal architecture and the loss of hepatocytes prevent the liver from its normal synthetic and metabolic function. Thus, the fibrogenic evolution progresses to cirrhosis, liver failure, and hepatocellular cancer.[2] There is increasing evidence that the hepatic fibrosis is reversible if the stimuli are successfully removed.[3] However, only subsets of liver diseases are treated effectively, and there are no specific treatments for liver fibrosis. An ideal anti-fibrogenic therapy would be liver-specific and effective in attenuating excessive ECM deposition.[4]

In all clinical and experimental liver fibrosis, myofibroblasts are the source of the ECM constituting the fibrous scar. Myofibroblasts are only found in the injured, but not the normal, liver. Thus, the activated myofibroblast is a pivotal player in development of liver cirrhosis, and has recently attracted interest as a therapeutic target. However, the origin of the hepatic myofibroblast is still unclear, and perhaps the fibrosis induced by different types of liver injury results from different fibrogenic cells. Hepatic myofibroblasts may originate from bone marrow-derived mesenchymal cells and fibrocytes,[5] but only a small contribution of BM derived cells to the myofibroblast population has been detected in experimental liver fibrosis. Another mechanism implicated in fibrogenesis is the epithelial-to-mesenchymal transition (EMT), in which epithelial cells acquire features of mesenchymal cells and may give rise to fully differentiated myofibroblasts.[6,7] However, recent cell fate mapping studies have failed to detect any hepatic myofibroblasts originating from hepatocytes, cholangiocytes, or epithelial progenitor cells. Endothelial-to-mesenchymal transition (EndMT), when endothelial cells undergo a similar phenotypic change to myofibroblasts[8,9] is a theoretically, but not yet assessed source of liver myofibroblasts. Thus, the major sources of myofibroblasts in liver fibrosis appear to be the endogenous liver mesenchymal cells, the hepatic stellate cells and the portal fibroblasts.

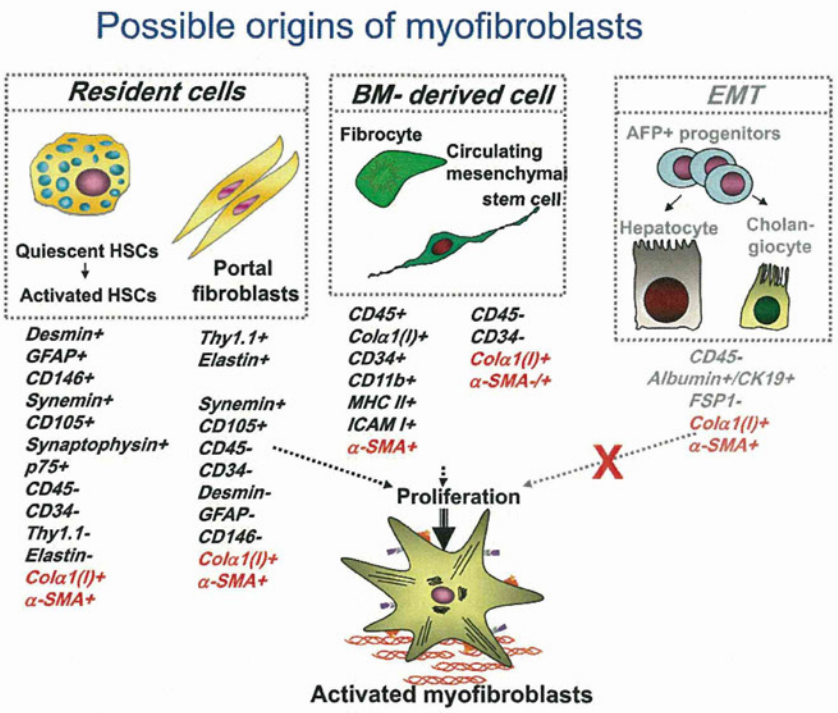

Figure 1 The proposed sources of hepatic myofibroblasts: resident cells (hepatic stellate cells and portal fibroblasts); bone marrow (BM)-derived mesenchymal cells, and cells originated by epithelial-to-mesenchymal transition. Modified from Bataller *et al.*[1]

Myofibroblasts

The origin of fibrogenic hepatic myofibroblasts has been intensively discussed and investigated, and several sources of myofibroblasts have been identified[10–13] (Fig. 1). In the fibrotic liver, hepatic stellate cells (HSCs) have been reported to mainly contribute to the collagen producing cells.[1] Therefore, HSCs are currently considered to be the major, but not the only, source of hepatic myofibroblasts in liver injury.[14]

Myofibroblasts are characterized by a stellate shape and expression of specific markers.[15] In response to fibrogenic stimuli, pro-fibrogenic cells are converted to myofibroblasts. They express α-smooth muscle actin (α-SMA), secrete ECM (e.g. collagen type I and III, fibronectin) and are highly contractile.[14] Classical myofibroblasts differentiate from a mesenchymal lineage and, therefore, lack expression of lymphoid markers such as CD45 or CD34.

The origins of myofibroblasts

Hepatic stellate cells

Hepatic stellate cells (HSCs) are perisinusoidal cells that normally reside in the space of Disse and have stored lipid droplets.[2,16] Under normal conditions, HSCs are present in the space of Disse and exhibit a quiescent phenotype. HSCs express neural markers, such as glial fibrilar acidic protein (GFAP), synemin, synaptophysin,[1] and nerve growth factor receptor p75,[17,18] desmin, secrete HGF, and store vitamin A in lipid droplets.[19] In response to chronic liver injury, quiescent HSCs are activated, release vitamin A and acquire contractility. Upon activation, HSCs change their morphology to become myofibroblasts, migrate to the site of injury, downregulate neural markers and upregulate mesenchymal markers, (e.g. collagen α1(I), α-SMA, and fibronectin).

Portal fibroblasts

Portal fibroblasts are spindle shaped cells that are present in the portal area. Under normal conditions, they participate in physiological ECM turnover[14,20–22] and do not express α-SMA. It is induced mostly by cholestatic liver injury,[23] that portal fibroblasts proliferate[24] and secrete collagen around portal tracts.[25] Portal fibroblasts are distinct from HSCs in that they do not have vitamin A droplets, but express elastin and Thy-1.1 (a glycophosphatidylinositol-linked glycoprotein of the outer membrane leaflet described in fibroblasts of several organs).[26,27] A proteomics study demonstrated that myofibroblasts derived from portal mesenchymal cells express much higher levels of cofilin-1 than activated HSCs. Portal fibroblasts do not express cytoglobin,[28] desmin or GFAP, so that these markers are useful to identify myofibroblasts derived from HSCs. In chronic cholestatic disorders, the fibrosis is initially located around portal tracts (Fig. 2). The histological findings of liver fibrosis combined with immunohistochemistry using these specific markers demonstrate that portal fibroblasts contribute to myofibroblasts in cholestatic liver injury.[1]

Born marrow derived mesenchymal cells

Born marrow (BM)-derived mesenchymal cells can also differentiate into myofibroblasts.[29,30] Myofbroblasts originated from BM-derived mesenchymal cells are seen in fibrotic lungs[31] and liver,[30] and contribute to fibrogenesis.[2,30,32] By fractionating the BM stem cell compartment, hepatic BM-derived mesenchymal stem cells (MSCs)[30,31] may differentiate into hepatic myofibroblasts. MSCs are defined as self-renewable, multipotent progenitor cells with the capacity to differentiate into lineage specific cells that form bone, cartilage, fat, tendon and muscle.[33,34] Unlike hematopoietic stem cells, MSCs are more radio-resistant[35] and reside mostly in

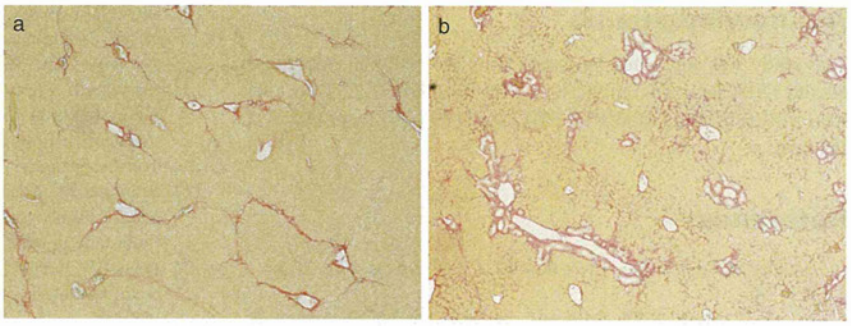

Figure 2 Liver fibrosis induced by hepatotoxic injury or cholestatic injury in mice. Liver sections were assessed by Sirius red staining. (a) Hepatotoxic injury model; the fibrotic tissue is initially located in pericentral and perisinusoidal areas. In advance, collagen bands to bridging fibrosis to frank cirrhosis occurs. (b) Cholestatic injury model; the fibrotic tissue is initially located around portal tracts.

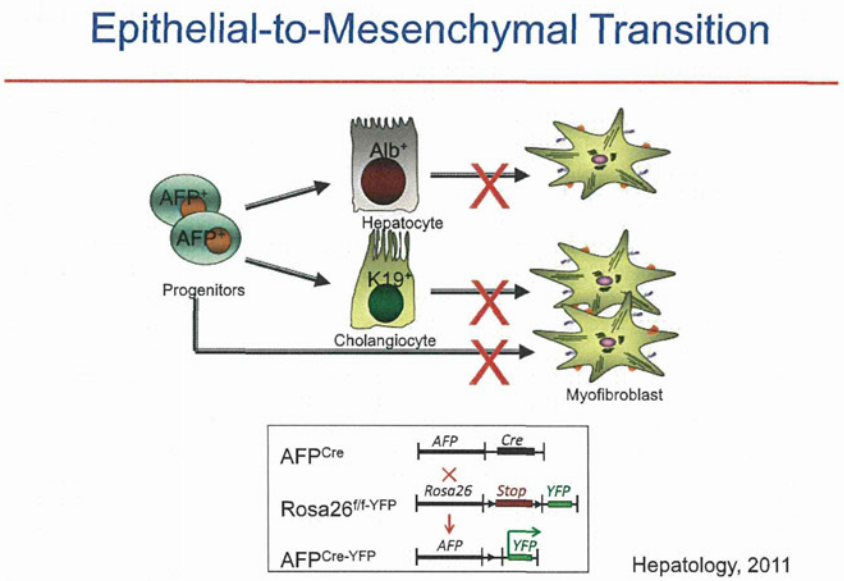

Figure 3 Analysis of epithelial-to-mesenchymal transition (EMT). (a) It is proposed that in EMT the myofibroblasts in liver fibrosis originate from hepatic epithelial cells, consisting of hepatocytes (albumin$^+$ [Alb$^+$] cells), cholangiocytes (cytokeratin-19$^+$ [K19$^+$] cells), or progenitor cells (AFP$^+$ cells). (b) Determining the origin of myofibroblasts using cell fate mapping. If a cell expressed α-fetoprotein (AFP), it will be irreversibly genetically labeled. AFP-driven Cre labeled epithelial progenitor cells, cholangiocytes, and hepatocytes, but failed to label any hepatic stellate cells (HSCs) or myofibroblasts. YFP, yellow fluorescent protein.[41]

BM stroma, do not express hematopoietic markers and can be isolated as Lin$^-$ CD45$^-$ CD31$^-$ CD34$^-$ CD133$^-$ Sca-1$^+$ Vitamin A$^-$ cells.[36,37] Whether BM-derived myofibroblasts contribute to ECM deposition in the course of liver fibrosis is unknown. In experimental liver fibrosis, only a small contribution of BM-derived cells to the myofibroblast population has been detected.[38]

Epithelial-to-mesenchymal transition

Epithelial-to-mesenchymal transition (EMT) is an important biological concept that describes the reversible transition of differentiated epithelial cells into mesenchymal cells with increased motility and changes in gene expression. Previous studies in the kidney and in the lung proposed that EMT occurs during fibrosis in those organs, and this concept was extrapolated to liver fibrosis.[39] Primary cell culture studies have clearly demonstrated that cholangiocytes and hepatocytes undergo a change in the phenotype and gene expression toward a mesenchymal cell, especially after incubation with transforming growth factor (TGF)-β, which is the cytokine most closely associated with EMT.[40] However, the more recent reports provide strong evidence against EMT in the liver as a source of myofibroblasts.[41] These studies use lineage tracing, such as by marking hepatic epithelial progenitor cells. Such mice are generated by crossing the α-fetoprotein (AFP) Cre mouse with the ROSA26YFP stop mouse to trace the fate of any cell ever expressing AFP. As expected, all cholangiocyutes, hepatocytes, and oval cells were genetically labeled, because they are derived from a common AFP-expressing precursor cell. Furthermore, the critical result was that after inducing liver fibrosis by a variety of methods, none of the resulting myofibroblasts originated from the genetically marked epithelial (AFP$^+$) cells (Fig. 3).

Conclusions

Myofibroblasts are the source of the fibrous scar in liver fibrosis. Hepatic myofibroblasts are transdifferentiated from heterogeneous cell populations in response to variety fibrogenic stimuli. According to the most recent studies, the major sources of hepatic myofibroblasts in experimental liver fibrosis are hepatic stellate cells and portal fibroblasts. The role of EMT in liver fibrosis has been recently questioned. As a first approximation, myofibroblasts generated in hepatotoxic liver injury appear to originate from HSCs and myofibroblasts generated in cholestatic liver injury may originate from portal fibroblasts (Fig. 2).

Acknowledgments

This study was supported by grants from the National Institute of Health (NIH RO1 DK090962-01, NIH RO1 DK072237-06, NIH RO1 GM041804-24, and NIH P50 AA011999-13) from David A. Brenner.

References

1 Bataller R, Brenner DA. Liver fibrosis. *J. Clin. Invest.* 2005; **115**: 209–18.
2 Iredale JP. Models of liver fibrosis: exploring the dynamic nature of inflammation and repair in a solid organ. *J. Clin. Invest.* 2007; **117**: 539–48.
3 Schnabl B, Scholten D, Brenner DA. What is the potential role of antifibrotic agents for the treatment of liver disease? *Nat. Clin. Pract. Gastroenterol. Hepatol.* 2008; **5**: 496–7.
4 Friedman SL, Bansal MB. Reversal of hepatic fibrosis—fact or fantasy? *Hepatology* 2006; **43**: S82–8.
5 Kisseleva T, Brenner DA. Fibrogenesis of parenchymal organs. *Proc. Am. Thorac. Soc.* 2008; **5**: 338–42.
6 Kalluri R. EMT: when epithelial cells decide to become mesenchymal-like cells. *J. Clin. Invest.* 2009; **119**: 1417–19.
7 Choi SS, Diehl AM. Epithelial-to-mesenchymal transitions in the liver. *Hepatology* 2009; **13**: 565–80.
8 Zeisberg EM, Tarnavski O, Zeisberg M *et al.* Endothelial-to-mesenchymal transition contributes to cardiac fibrosis. *Nat. Med.* 2007; **13**: 952–61.
9 Zeisberg EM, Potenta SE, Sugimoto H, Zeisberg M, Kalluri R. Fibroblasts in kidney fibrosis emerge via endothelial-tomesenchymal transition. *J. Am. Soc. Nephrol.* 2008; **19**: 2282–7.
10 Kisseleva T, Brenner DA. Hepatic stellate cells and the reversal of fibrosis. *J. Gastroenterol. Hepatol.* 2006; **21** (Suppl. 3): S84–7.
11 Kalluri R, Neilson EG. Epithelial-mesenchymal transition and its implications for fibrosis. *J. Clin. Invest.* 2003; **112**: 1776–84.
12 Gomperts BN, Strieter RM. Fibrocytes in lung disease. *J. Leukoc. Biol.* 2007; **82**: 449–56.
13 Fallowfield JA, Mizuno M, Kendall TJ *et al.* Scar-associated macrophages are a major source of hepatic matrix metalloproteinase-13 and facilitate the resolution of murine hepatic fibrosis. *J. Immunol.* 2007; **178**: 5288–95.
14 Parola M, Marra F, Pinzani M. Myofibroblast—like cells and liver fibrogenesis: emerging concepts in a rapidly moving scenario. *Mol. Aspects Med.* 2008; **29**: 58–66.
15 Eyden B. The myofibroblast: phenotypic characterization as a prerequisite to understanding its functions in translational medicine. *J. Cell. Mol. Med.* 2008; **12**: 22–37.
16 Geerts A. History, heterogeneity, developmental biology, and functions of quiescent hepatic stellate cells. *Semin. Liver Dis.* 2001; **21**: 311–35.
17 Sachs BD, Baillie GS, McCall JR *et al.* p75 neurotrophin receptor regulates tissue fibrosis through inhibition of plasminogen activation via a PDE4/cAMP/PKA pathway. *J. Cell Biol.* 2007; **177**: 1119–32.
18 Kendall TJ, Hennedige S, Aucott RL *et al.* p75 Neurotrophin receptor signaling regulates hepatic myofibroblast proliferation and apoptosis in recovery from rodent liver fibrosis. *Hepatology* 2009; **49**: 901–10.
19 Senoo H, Kojima N, Sato M. Vitamin a-storing cells (stellate cells). *Vitam. Horm.* 2007; **75**: 131–59.
20 Tuchweber B, Desmouliere A, Bochaton-Piallat ML, Rubbia-Brandt L, Gabbiani G. Proliferation and phenotypic modulation of portal fibroblasts in the early stages of cholestatic fibrosis in the rat. *Lab. Invest.* 1996; **74**: 265–78.
21 Guyot C, Lepreux S, Combe C *et al.* Hepatic fibrosis and cirrhosis: the (myo) fibroblastic cell subpopulations involved. *Int. J. Biochem. Cell Biol.* 2006; **38**: 135–51.
22 Kinnman N, Francoz C, Barbu V *et al.* The myofibroblastic conversion of peribiliary fibrogenic cells distinct from hepatic stellate cells is stimulated by platelet-derived growth factor during liver fibrogenesis. *Lab. Invest.* 2003; **83**: 163–73.
23 Beaussier M, Wendum D, Schiffer E *et al.* Prominent contribution of portal mesenchymal cells to liver fibrosis in ischemic and obstructive cholestatic injuries. *Lab. Invest.* 2007; **87**: 292–303.
24 Wells RG, Kruglov E, Dranoff JA. Autocrine release of TGF-beta by portal fibroblasts regulates cell growth. *FEBS Lett.* 2004; **559**: 107–10.
25 Knittel T, Kobold D, Saile B *et al.* Rat liver myofibroblasts and hepatic stellate cells: different cell populations of the fibroblast lineage with fibrogenic potential. *Gastroenterology* 1999; **117**: 1205–21.
26 Dudas J, Mansuroglu T, Batusic D, Saile B, Ramadori G. Thy-1 is an *in vivo* and *in vitro* marker of liver myofibroblasts. *Cell Tissue Res.* 2007; **329**: 503–14.
27 Yovchev MI, Zhang J, Neufeld DS, Grozdanov PN, Dabeva MD. Thymus cell antigen-1-expressing cells in the oval cell compartment. *Hepatology* 2009; **50**: 601–11.
28 Bosselut N, Housset C, Marcelo P *et al.* Distinct proteomic features of two fibrogenic liver cell populations: hepatic stellate cells and portal myofibroblasts. *Proteomics* 2010; **10**: 1017–28.
29 Forbes SJ, Russo FP, Rey V *et al.* A significant proportion of myofibroblasts are of bone marrow origin in human liver fibrosis. *Gastroenterology* 2004; **126**: 955–63.
30 Russo FP, Alison MR, Bigger BW *et al.* The bone marrow functionally contributes to liver fibrosis. *Gastroenterology* 2006; **130**: 1807–21.
31 Hashimoto N, Jin H, Liu T, Chensue SW, Phan SH. Bone marrow-derived progenitor cells in pulmonary fibrosis. *J. Clin. Invest.* 2004; **113**: 243–52.
32 Kisseleva T, Brenner DA. Mechanisms of fibrogenesis. *Exp. Biol. Med. (Maywood)* 2008; **233**: 109–22.
33 Kallis YN, Forbes SJ. The bone marrow and liver fibrosis: friend or foe? *Gastroenterology* 2009; **137**: 1218–21.
34 Song L, Tuan RS. Transdifferentiation potential of human mesenchymal stem cells derived from bone marrow. *FASEB J.* 2004; **18**: 980–2.
35 Bartsch K, Al-Ali H, Reinhardt A *et al.* Mesenchymal stem cells remain host-derived independent of the source of the stem-cell graft and conditioning regimen used. *Transplantation* 2009; **87**: 217–21.
36 Short BJ, Brouard N, Simmons PJ. Prospective isolation of mesenchymal stem cells from mouse compact bone. *Methods Mol. Biol.* 2009; **482**: 259–68.
37 Simmons PJ, Przepiorka D, Thomas ED, Torok-Storb B. Host origin of marrow stromal cells following allogeneic bone marrow transplantation. *Nature* 1987; **328**: 429–32.
38 Kisseleva T, Uchinami H, Feirt N *et al.* Bone marrow-derived fibrocytes participate in pathogenesis of liver fibrosis. *J. Hepatol.* 2006; **45**: 429–38.
39 Zeisberg M, Duffield JS. Resolved: EMT produces fibroblasts in the kidney. *J. Am. Soc. Nephrol.* 2010; **21**: 1247–53.
40 Taura K, Miura K, Iwaisako K *et al.* Hepatocytes do not undergo epithelial-mesenchymal transition in liver fibrosis in mice. *Hepatology* 2010; **51**: 1027–36.
41 Chu AS, Diaz R, Hui JJ *et al.* Lineage tracing demonstrates no evidence of cholangiocyte epithelial-to-mesenchymal transition in murine models of hepatic fibrosis. *Hepatology* 2011; **53**: 1685–95.